TECHNICAL PAPER

CrossMark

Nanoscale mass nanosensor based on the vibration analysis of embedded magneto-electro-elastic nanoplate made of FGMs via nonlocal Mindlin plate theory

M. Hosseini[1] · M. R. Mofidi[1] · A. Jamalpoor[2] · M. Safi Jahanshahi[1]

Abstract

In the current paper, the sensitivity performance of functionally graded magneto-electro-elastic (FG-MEE) nanoplate with attached nanoparticles as a nanosensor is analyzed based on nonlocal Mindlin plate assumption. Power law distribution model is employed to display how the material properties of FG-MEE nanoplate vary across the thickness direction. It is supposed that FG-MEE nanoplate is under initial external electric and magnetic potentials. Boundary condition of each edge of FG-MEE nanoplate is assumed to be simply supported. Furthermore, a Pasternak substrate is applied for modelling the total reaction pressure between nanoplate and foundation. Partial differential equations and corresponding boundary conditions are first achieved using Hamilton's variational principle and then analytically solved to determine the frequency shift utilizing Navier's approach. Numerical examples are performed to elucidate the dependency of the sensitivity performance of FG-MEE nanosensor on the volume fraction exponent, nonlocal parameter, total attached mass and location of the nanoparticle, aspect ratio, mode number, initial external electric voltage, initial external magnetic potential, and Pasternak medium coefficients. It is clearly indicated that these factors have highly significant impacts on the variations of frequency shift.

1 Introduction

In the recent years, with the rapid growth in the use of the composite materials in a wide range of engineering structures such as aircraft structures (Baker and Baker 2004) and sensor and actuators (Tressler et al. 1999; Akdogan et al. 2005; Li et al. 2008) because of their excellent mechanical properties, the importance of recognizing the composite material behavior increases day to day. Magneto-electro-elastic (MEE) composite materials are an important class of smart composite materials combining piezoelectric and piezomagnetic phases. The capacity of converting energy among magnetism, electricity, or elasticity into another form has caused that the MEE materials become suitable for smart applications. Up to now, various

analytical or numerical works have been carried out to investigate MEE plate, beam, and shell which contain studies on the static behavior (Wu and Tsai 2007; Wu et al. 2010), linear and nonlinear vibration (Ramirez et al. 2006; Razavi and Shooshtari 2015; Shirbani et al. 2017) and on the post-buckling behavior (Zhou et al. 2003). For the first time, the excellent behavior of MEE composite materials experimentally was reported by Van Den Boomgaard et al. (1974). A discrete layer model is applied to predict the natural frequencies of orthotropic functionally graded (FG) MEE plates combining various percentages of barium titanate ($BaTiO_3$) and cobalt iron oxide ($CoFe_2O_4$) by Ramirez et al. (2006). Nonlinear forced vibration of a MEE plate is investigated via first-order shear deformation theory by Shooshtari and Razavi (2016). Liu et al. (2016) developed a MEE 3D model for studying the components of the MEE field. Surface effects include surface piezoelectricity, surface elasticity and surface piezomagneticity investigated on the bending, buckling and free vibration of the MEE Euler–Bernoulli beams by Xu et al. (2016).

During the recent years, the investigation of the mechanical behavior of MEE structures at nano- and micro- scales have attracted the interest of some

✉ M. Hosseini
  hosseini@sirjantech.ac.ir

[1] Department of Mechanical Engineering, Sirjan University of Technology, Sirjan 78137-33385, Iran

[2] Department of Mechanical Engineering, Iran University of Science and Technology, Narmak, Tehran 16846-13114, Iran

Fig. 1 The geometry of FG-MEE nanoplate with multiple attached nanoparticle resting on Pasternak medium (color figure online)
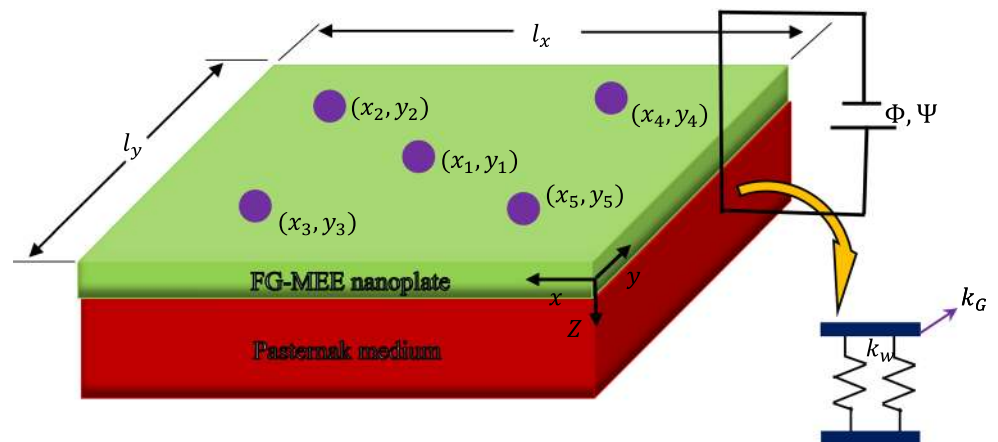
researchers. It have proven that the classical approaches cannot predict satisfactorily the mechanical behavior of nano- and micro- structures (Pradhan and Phadikar 2009; Ansari et al. 2010; Hosseini et al. 2016a, b, c). Experiments and atomistic simulations (Chen et al. 2006; Stan et al. 2007) demonstrated that the influence of small size becomes significant when the dimensions of the structure become small and reach to the micro/nano length scale. Since the traditional classical elasticity and plasticity theories have no material internal length scale, these theories are not capable of taking into account the influence of small size scale. Therefore, these theories modified and included one or several independent internal length scale parameters. Some of the most popular modified theories include nonlocal elasticity theory suggested by Eringen (1972, 1983), modified couple stress theory presented (MCST) by Yang et al. (2002) and modified strain gradient theory (MSGT) suggested by Lam et al. (2003).

Our literature review here will focus on the analysis of MEE nanostructures based on the nonlocal elasticity of Eringen. According to the suggested model of Eringen, the elastic strain is described by a Fredholm type integral equations in which the stress is result of a convolution between the local response to an elastic strain and a smoothing kernel dependent on a nonlocal parameter. But some researchers showed the constitutive boundary conditions and paradoxes of nonlocal integral model (Romano and Barretta 2016, 2017a, b; Romano et al. 2017a, b;

Apuzzo et al. 2017). They demonstrated that Eringen's nonlocal integral model admits no solution. On the basis of the nonlocal elasticity theory of Eringen, Ansari et al. (2015c) proposed a third-order shear deformable beam model to study forced vibration behavior of magneto-electro-thermo-elastic nanobeams by taking into account the effects of small scale. Recently, by considering the von Kármán's assumption, the influences of the external electric and magnetic potential on the nonlinear natural frequencies of the MEE nanoplates are shown by Farajpour et al. (2016). Wang et al. (2016) presented a novel two-dimensional linear elastic theory for demonstrating surface, nonlocal effects, poling directions, piezoelectric phase materials on the MEE nanoplate. Numerical results illustrated that driving frequency and output power density of magnetic energy harvesters have obvious size-dependent behavior because of surface effects. On the basis of the nonlocal Mindlin plate approach, Li et al. (2014) analytically carried out elastic instability and free vibration behavior of MEE nanoplate resting on Pasternak medium. It was shown that buckling load and natural frequency decrease (increase) linearly with electric potential (magnetic potential). Recently, the generalized differential quadrature method in conjunction with pseudo arc-length continuation are applied to calculate the nonlinear buckling and postbuckling of MEE Mindlin nanoplate under thermal load by Ansari and Gholami (2017). A mathematical model based on Euler–Bernoulli beam assumption is proposed by

Table 1 Comparison study of the first two dimensionless natural frequencies of MEE nanoplate

|		$\mu = 0$	$\mu = 0.2$	$\mu = 0.4$
ω_{11}	KPT (Ke et al. 2014)	0.3698	0.2764	0.1813
	MPT(DQM) (Ansari and Gholami 2016)	0.3684	0.2756	0.1808
	Present	0.3683	0.2755	0.1806
ω_{12}	KPT (Ke et al. 2014)	0.9247	0.5362	0.3100
	MPT(DQM) (Ansari and Gholami 2016)	0.9108	0.5284	0.3055
	Present	0.9107	0.5283	0.3053

Vaezi et al. (2016) for investigating natural frequencies and buckling loads of MEE microbeam. Moreover, there are a number of literatures regarding the influences of small scale on the MEE nanostructures such as MEE nanobeams (Ke and Wang 2014; Ansari et al. 2015b; Li et al. 2016; Ma et al. 2017) and MEE nanoplates (Ke et al. 2014; Wu et al. 2015; Jamalpoor et al. 2017; Kiani et al. 2017) by taking into account the nonlocal parameter.

Functionally graded materials (FGMs) are a special subgroup of novel composite materials which contain the heterogeneous property and have a continuous variation of material properties from one surface to another. Due to the numerous profits containing high mechanical and thermal resistance, FGMs are vastly used in sensors and thermo-generators (Müller et al. 2003; Rahimi et al. 2011), biomedical fields (Pompe et al. 2003; Parthasarathy et al. 2011), aerospace (Kumar et al. 2013). With respect to the development of science and wide application of FGM nanostructures, the study of the size effect on the mechanical behavior of FGM nanostructures is of considerable practical interest. On the basis of nonlocal elasticity theory in conjunction with Gurtin–Murdoch elasticity theory, Hosseini and Jamalpoor (2015) reported the important role of the surface effects, i.e., surface elasticity, residual stresses and surface density on the free vibration of a double-FGM viscoelastic nanoplates-system under thermal load. They considered that the material traits of the plate follow power law repartition in the thickness direction.

Numerical results expressed that an increase in the amount of the power law index makes a reduction of the natural frequencies. A modified power-law model in conjunction with the refined four-variable plate assumption are implemented by Barati et al. (2017) to study the influence of FGMs on the vibration frequency of smart piezoelectric plates under various boundary conditions. Wave propagation phenomena of a FG-MEE nanorod is investigated via nonlocal continuum mechanics by Narendar (2016). Furthermore, there are a number of literatures regarding the effects of FGMs on the nanostructures (Natarajan et al. 2012; Ansari et al. 2015a; Barretta et al. 2016; Thang et al. 2017; Mechab et al. 2016; Jamalpoor and Kiani 2017; Hosseini et al. 2017).

It should be pointed that sometimes one or more concentrated particles are attached to the structures. Thus, we need the mass detection technology for detecting the position of attached masses with high accuracy and sensitivity. In order to find the exact point of attached masses, sensors play a significant role. The main idea for determining the location of added masses such as bacterium/virus, biomolecules, and buckyballs is to measure the resonant frequency shift of the nanosensor caused by variations in total mass of the system (Zhou et al. 2014; Asemi et al. 2015; Karličić et al. 2015; Shi et al. 2015; Jalali et al. 2015; Sadeghzadeh 2016). It is that piezoelectric (ZnO-BaTiO$_3$) (Guo et al. 2012; Alluri et al. 2015), magnetic/piezoelectric (Yeh et al. 2016), and magnetic (CoFe$_2$O$_4$)

Fig. 2 Comparison study between the fundamental frequency shift predicted by present model and those reported in Ref. Asemi et al. (2015) (color figure online)
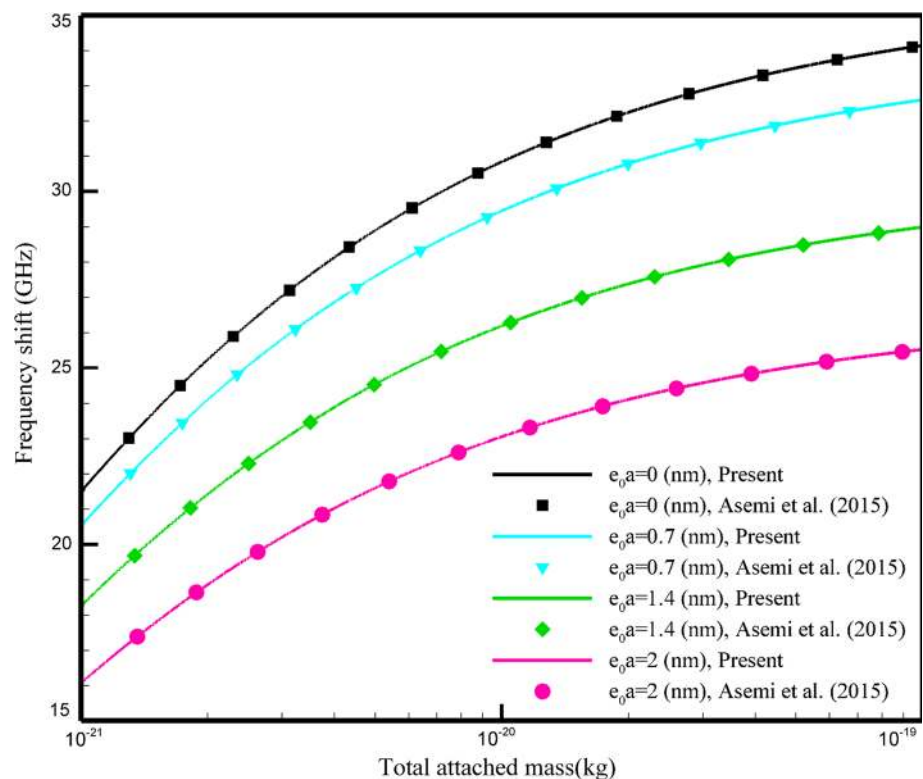
(Kim et al. 2009; Taei et al. 2016) can be suitable candidates for sensor devices because of having excellent properties like dimensional stability, abrasion, and corrosion resistance.

The above-reviewed papers explicitly illustrated that while there exist a considerable number of studies that deal with the static and dynamic responses of MEE nanoplate based on different (Kirchhoff or Mindlin) plate assumptions, nanoscale mass detection based on vibration FG-MEE Mindlin nanoplate seem to be nonexistent. Accordingly, in this work, a first-order shear deformable (Mindlin) plate theory in conjunction with the nonlocal elasticity theory is applied to take into account the size effect on the sensitivity of the sensor. In this regard, the key novelties of the presented study are summarized as follows:

- Development of a nonlocal Mindlin plate theory for free vibration of FG-MEE nanoplate resting on the Pasternak medium.
- FG-MEE Mindlin nanoplate with attached concentrated nanoparticles is presented as a mass nanosensor according to the vibration analysis.

Partial differential equations of motion of the system with multiple added masses are derived by employing Hamilton's principle, then by applying the analytical Navier type solution, the frequency shift of the system is presented in the explicit closed-form.

2 Modeling of problem and formulation

2.1 Geometrical configuration

Consider a simply supported thick rectangular $(l_x \times l_y)$ nanoplate with uniform thickness h consisting of $BaTiO_3$-$CoFe_2O_4$ MEE, which is exposed to electric $\Phi(x, y, z, t)$ and magnetic potentials $\Psi(x, y, z, t)$, as shown in Fig. 1. As can be seen from Fig. 1, it is considered that nanoplate with

attached nanoparticles is resting on the Pasternak-type foundation with the transverse and shear coefficients k_w and k_G, respectively. Also, the location of any rigid nanoparticle is assumed to be at $(x_e, y_e), e = 1, 2, \ldots$. Furthermore, the material properties of MEE nanoplate are supposed to be graded in the thickness direction based on the power-law model in terms of the volume fractions of the constituents. It should be noted that in FG-MEE nanoplate, the materials properties vary continuously from a fully $BaTiO_3$ phase at the top surface $(z = \frac{h}{2})$ to a fully $CoFe_2O_4$ phase at the bottom surface $(z = -\frac{h}{2})$.

2.2 Constitutive relations for nonlocal FG-MEE Mindlin nanoplate

2.2.1 FGMs

On the basis of the power law distribution, the effective material characteristics of MEE nanoplate vary continuously across the plate thickness and can be proposed as below:

$$PM(z) = PM_2 V_2 + PM_1 V_1 \tag{1}$$

where, PM_1 and PM_2 are the properties of $CoFe_2O_4$ phase and $BaTiO_3$ phase, respectively. Also, V_1 and V_2 refer to the volume fractions of $CoFe_2O_4$ rich and $BaTiO_3$ rich, respectively, which can be written as

$$V_2 = \left(\frac{1}{2} + \frac{z}{h}\right)^K, \quad V_1 = 1 - V_2 \tag{2}$$

in which K is the volume fraction exponent and always has a positive value.

2.2.2 Displacement field

In order to obtain more accurate estimation of mechanical behavior of thick plate, we apply Mindlin plate hypothesis (first-order shear deformation theory) which incorporates

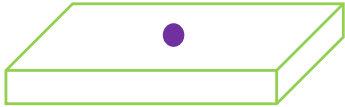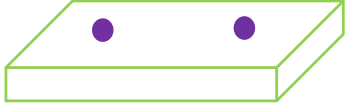Table 2 The details of the three different configurations of attached nanoparticles

Pictorial representation	m_{Total}	Position (X_e, Y_e)
	$m_1 = m_{Total}$	$(0.5, 0.5)$
	$m_1 = \frac{m_{Total}}{2}$	$(0.25, 0.5)$
	$m_2 = \frac{m_{Total}}{2}$	$(0.75, 0.5)$
	$m_1 = \frac{m_{Total}}{4}$	$(0.25, 0.25)$
	$m_2 = \frac{m_{Total}}{4}$	$(0.25, 0.75)$
	$m_3 = \frac{m_{Total}}{4}$	$(0.75, 0.25)$
	$m_4 = \frac{m_{Total}}{4}$	$(0.75, 0.75)$

Table 3 Material properties of MEE (physical constants are set in italic type and their units are given in parentheses)

Properties	BaTiO$_3$	CoFe$_2$O$_4$
C_{11} (GPa)	166	286
C_{12}	77	173
C_{13}	78	170.5
C_{22}	166	286
C_{23}	78	170.5
C_{33}	162	269.5
C_{44}	43	45.3
C_{55}	43	45.3
C_{66}	44.5	56.5
e_{31} (C/m^2)	− 4.4	0
e_{32}	− 4.4	0
e_{24}	11.6	0
e_{15}	11.6	0
e_{33}	18.6	0
q_{31} (N/Am)	0	580.3
q_{32}	0	580.3
q_{24}	0	550
q_{15}	0	550
q_{33}	0	699.7
η_{11} (10^{-9} C^2/Nm^2)	11.2	0.08
η_{22}	11.2	0.08
η_{33}	12.6	0.093
d_{11} (s/m)	0	0
d_{22}	0	0
d_{33}	0	0
μ_{11} (10^{-6} Ns^2/C^2)	5	− 590
μ_{22}	5	− 590
μ_{33}	10	157
ρ (kg/m^3)	5800	5300

the shear deformations through-the-thickness of a plate into classical plate theory. On the basis of Mindlin plate theory, the displacement fields of the plate can be proposed in the five unknown parameters in Cartesian coordinate as below

$$
\begin{aligned}
u_x(x, y, z, t) &= u_0(x, y, t) + z\theta_x(x, y, t) \\
u_y(x, y, z, t) &= v_0(x, y, t) + z\theta_y(x, y, t) \\
u_z(x, y, z, t) &= w_0(x, y, t)
\end{aligned}
\tag{3}
$$

in which u_0 and v_0 denote the in plane deflections of the mid-surface; θ_x and θ_y refer to the rotation of the middle plane in the x and y directions, respectively; and w_0 is the lateral displacement.

2.2.3 Strains

The nonzero components of the linear strain–displacement relationships can be expressed as

$$
\begin{aligned}
\varepsilon_{xx} &= \frac{\partial u_0}{\partial x} + z\frac{\partial \theta_x}{\partial x} \\
\varepsilon_{yy} &= \frac{\partial v_0}{\partial y} + z\frac{\partial \theta_y}{\partial y} \\
\gamma_{xz} &= \theta_x + \frac{\partial w_0}{\partial x} \\
\gamma_{yz} &= \theta_y + \frac{\partial w_0}{\partial y} \\
\gamma_{xy} &= \frac{\partial u_0}{\partial y} + \frac{\partial v_0}{\partial x} + z\left(\frac{\partial \theta_x}{\partial y} + \frac{\partial \theta_y}{\partial x}\right)
\end{aligned}
\tag{4}
$$

2.3 Nonlocal elasticity theory

It is considered via Eringen's nonlocal elastic theory (Eringen 1972, 1983) that the stress, electric displacement, and magnetic induction at a reference spot of MEE nanostructures are supposed to be a function of the strain, electric and magnetic components at each spot in material domain of body. According to the main idea of this nonlocal theory, the basic relations for FG-MEE substance without considering body force can be written as follows (Ansari et al. 2015b; Farajpour et al. 2016)

$$
\begin{aligned}
\sigma_{ij}^{nl} &= \int \mathcal{F}\left(|x - x'|, \frac{e_0 a}{b}\right)\sigma_{ij}^{l} dV(x'), \forall x \int V, \\
D_i^{nl} &= \int \mathcal{F}\left(|x - x'|, \frac{e_0 a}{b}\right)D_i^{l} dV(x'), \forall x \int V, \\
B_i^{nl} &= \int \mathcal{F}\left(|x - x'|, \frac{e_0 a}{b}\right)B_i^{l} dV(x'), \forall x \int V, \\
\sigma_{ij}^{l} &= \bar{C}_{iikl}(z)\varepsilon_{kl}(x') - \bar{e}_{mij}(z)E_m(x') - \bar{q}_{nij}(z)H_n(x'), \\
D_i^{l} &= \bar{e}_{ikl}(z)\varepsilon_{kl}(x') + \bar{\eta}_{im}(z)E_m(x') + \bar{d}_{in}(z)H_n(x'), \\
B_i^{l} &= \bar{q}_{ikl}(z)\varepsilon_{kl}(x') + \bar{d}_{im}(z)E_m(x') + \bar{\mu}_{in}(z)H_n(x'),
\end{aligned}
\tag{5}
$$

where the terms $\sigma_{ij}^{nl} = \begin{bmatrix} \sigma_{xx}^{nl} & \sigma_{yy}^{nl} & \sigma_{yz}^{nl} & \sigma_{xz}^{nl} & \sigma_{xy}^{nl} \end{bmatrix}^T$, $D_i^{nl} = \begin{bmatrix} D_x^{nl} & D_y^{nl} & D_z^{nl} \end{bmatrix}^T$ and $B_i^{nl} = \begin{bmatrix} B_x^{nl} & B_y^{nl} & B_z^{nl} \end{bmatrix}^T$ (the superscript T signifies transpose) represent, respectively, the nonlocal forms of the stress tensor, electric displacement and magnetic induction. Also, σ_{ij}^{l}, D_i^{l} and B_i^{l} demonstrate, respectively, the local forms of the stress tensor, electric displacement and magnetic induction. $\mathcal{F}\left(|x - x'|, \frac{e_0 a}{b}\right)$ indicates the Kernel function, and the Euclidean distance between reference point x and any points x' in the body is illustrated with the symbol $|x - x'|$. Furthermore, in Eq. (5), E_m and H_n are electric field and magnetic field vectors, respectively. Also, symbol V is the volume of MEE

Table 4 The effect of length to thickness ratio and material property gradient index on the changes of frequency shift

$\frac{l_x}{h}$	Number of mass	Power law index, K				
		Fully BaTiO$_3$	0.5	1	10	Fully CoFe$_2$O$_4$
5	Single mass	0.5600	0.5937	0.6020	0.6341	0.6494
	Two masses	0.5090	0.5401	0.5482	0.5785	0.5905
	Four masses	0.4413	0.4697	0.4773	0.5052	0.5162
10	Single mass	0.2428	0.2604	0.2656	0.2828	0.2896
	Two masses	0.1979	0.2129	0.2175	0.2326	0.2384
	Four masses	0.1480	0.1599	0.1637	0.1760	0.1805
15	Single mass	0.1292	0.1393	0.1425	0.1528	0.1567
	Two masses	0.0952	0.1031	0.1056	0.1138	0.1169
	Four masses	0.0633	0.0689	0.0708	0.0767	0.0788

substance. Nonlocal parameter that takes into account the small scale effects into the constitutive equations is demonstrated by $\frac{e_0 a}{b}$, which e_0 is a constant parameter determined experimentally for matching theoretical model with empirical results; a is the internal characteristic length (e.g. lattice parameter, granular size); and b refers to an external property of length (e.g. crack length, wavelength). However, the strain-driven integral constitutive nonlocal relation (5) proposed by Eringen (1983) is inapplicable to nonlocal elastic problems on bounded structural domains (Romano and Barretta 2016, 2017a, b; Romano et al. 2017a, b; Apuzzo et al. 2017). In this paper we assume the following phenomenological differential constitutive law (consequent but not equivalent to Eq. 5) to investigate size-dependent behavior of Mindlin plates.

$$\left[1-(e_0 a)^2 \nabla^2\right]\begin{bmatrix} \sigma_{xx}^{nl} \\ \sigma_{yy}^{nl} \\ \sigma_{yz}^{nl} \\ \sigma_{xz}^{nl} \\ \sigma_{xy}^{nl} \end{bmatrix} = [\bar{C}(z)]\begin{bmatrix} \varepsilon_{xx} \\ \varepsilon_{yy} \\ \gamma_{yz} \\ \gamma_{xz} \\ \gamma_{xy} \end{bmatrix} - [\bar{e}(z)]\begin{bmatrix} E_x \\ E_y \\ E_z \end{bmatrix} - [\bar{q}(z)]\begin{bmatrix} H_x \\ H_y \\ H_z \end{bmatrix},$$

$$\left[1-(e_0 a)^2 \nabla^2\right]\begin{bmatrix} D_x^{nl} \\ D_y^{nl} \\ D_z^{nl} \end{bmatrix} = [\bar{e}(z)]^T\begin{bmatrix} \varepsilon_{xx} \\ \varepsilon_{yy} \\ \gamma_{yz} \\ \gamma_{xz} \\ \gamma_{xy} \end{bmatrix} + [\bar{\eta}(z)]\begin{bmatrix} E_x \\ E_y \\ E_z \end{bmatrix} + [\bar{d}(z)]\begin{bmatrix} H_x \\ H_y \\ H_z \end{bmatrix},$$

$$\left[1-(e_0 a)^2 \nabla^2\right]\begin{bmatrix} B_x^{nl} \\ B_y^{nl} \\ B_z^{nl} \end{bmatrix} = [\bar{q}(z)]^T\begin{bmatrix} \varepsilon_{xx} \\ \varepsilon_{yy} \\ \gamma_{yz} \\ \gamma_{xz} \\ \gamma_{xy} \end{bmatrix} + [\bar{d}(z)]\begin{bmatrix} E_x \\ E_y \\ E_z \end{bmatrix} + [\bar{\mu}(z)]\begin{bmatrix} H_x \\ H_y \\ H_z \end{bmatrix},$$

(6)

in which $\nabla^2 = \frac{\partial^2}{\partial x^2} + \frac{\partial^2}{\partial y^2}$ denotes the two-dimensional Laplacian operator. By not considering the size effect ($e_0 a = 0$), the traditional classical constitutive relations of FG-MEE structures can be acquired from nonlocal basic relations. $[\bar{C}]$, $\bar{e}$, $[\bar{q}]$, $\bar{\eta}$, $[\bar{d}]$ and $[\bar{\mu}]$ denote, respectively, the elastic, piezoelectric, piezomagnetic, dielectric,

magnetoelectric and magnetic constant matrices, which here are supposed to be varied continuously as a power law function of the plate thickness and are illustrated as below

$$[\bar{C}(z)] = \begin{bmatrix} \bar{C}_{11}(z) & \bar{C}_{12}(z) & 0 & 0 & 0 \\ \bar{C}_{12}(z) & \bar{C}_{22}(z) & 0 & 0 & 0 \\ 0 & 0 & \bar{C}_{44}(z) & 0 & 0 \\ 0 & 0 & 0 & \bar{C}_{55}(z) & 0 \\ 0 & 0 & 0 & 0 & \bar{C}_{66}(z) \end{bmatrix},$$

$$[\bar{e}(z)] = \begin{bmatrix} 0 & 0 & \bar{e}_{31}(z) \\ 0 & 0 & \bar{e}_{32}(z) \\ 0 & \bar{e}_{24}(z) & 0 \\ \bar{e}_{15}(z) & 0 & 0 \\ 0 & 0 & 0 \end{bmatrix},$$

$$[\bar{q}(z)] = \begin{bmatrix} 0 & 0 & \bar{q}_{31}(z) \\ 0 & 0 & \bar{q}_{32}(z) \\ 0 & \bar{q}_{24}(z) & 0 \\ \bar{q}_{15}(z) & 0 & 0 \\ 0 & 0 & 0 \end{bmatrix},$$

$$[\bar{\eta}(z)] = \begin{bmatrix} \bar{\eta}_{11}(z) & 0 & 0 \\ 0 & \bar{\eta}_{22}(z) & 0 \\ 0 & 0 & \bar{\eta}_{33}(z) \end{bmatrix},$$

$$[\bar{d}(z)] = \begin{bmatrix} \bar{d}_{11}(z) & 0 & 0 \\ 0 & \bar{d}_{22}(z) & 0 \\ 0 & 0 & \bar{d}_{33}(z) \end{bmatrix},$$

$$[\bar{\mu}(z)] = \begin{bmatrix} \bar{\mu}_{11}(z) & 0 & 0 \\ 0 & \bar{\mu}_{22}(z) & 0 \\ 0 & 0 & \bar{\mu}_{33}(z) \end{bmatrix}.$$

(7)

By supposing the plane stress state, the reduced material constants $\bar{C}_{ij}(z), \bar{e}_{ij}(z), \bar{q}_{ij}(z), \bar{\eta}_{ij}(z), \bar{d}_{ij}(z)$ and $\bar{\mu}_{ij}(z)$ can be denoted as follows

Fig. 3 Coupled effects of the nonlocal parameter and number of added nanoparticles on the fundamental frequency shift versus different values of the total attached mass (color figure online)
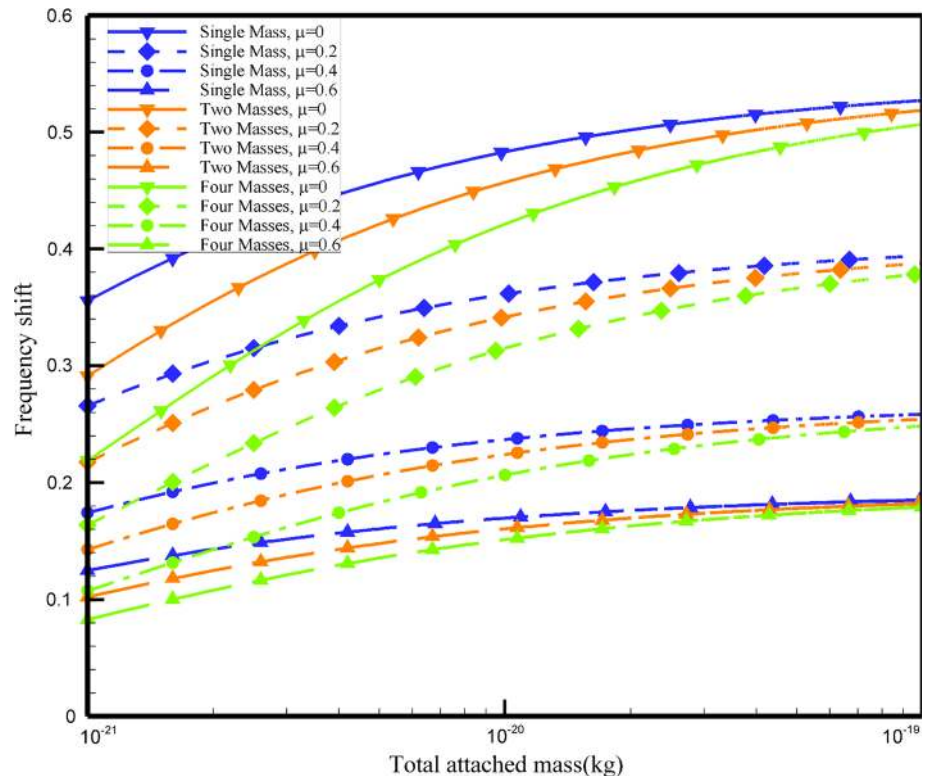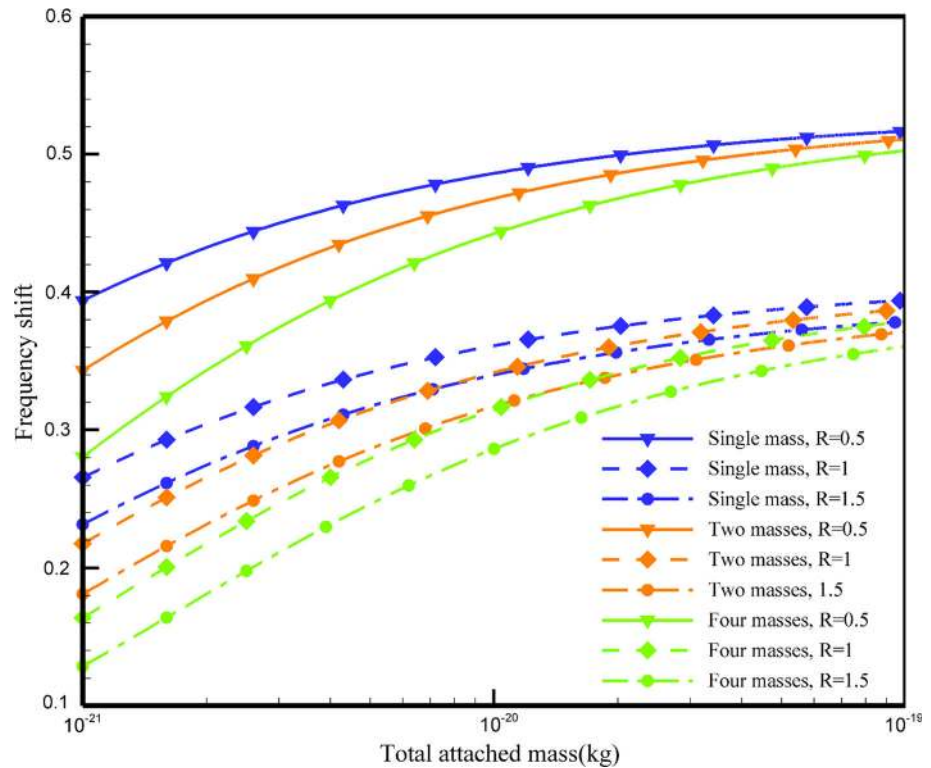

Fig. 4 Changes of the fundamental frequency shift of nanosensor as a function of total attached mass for various values of aspect ratio (color figure online)
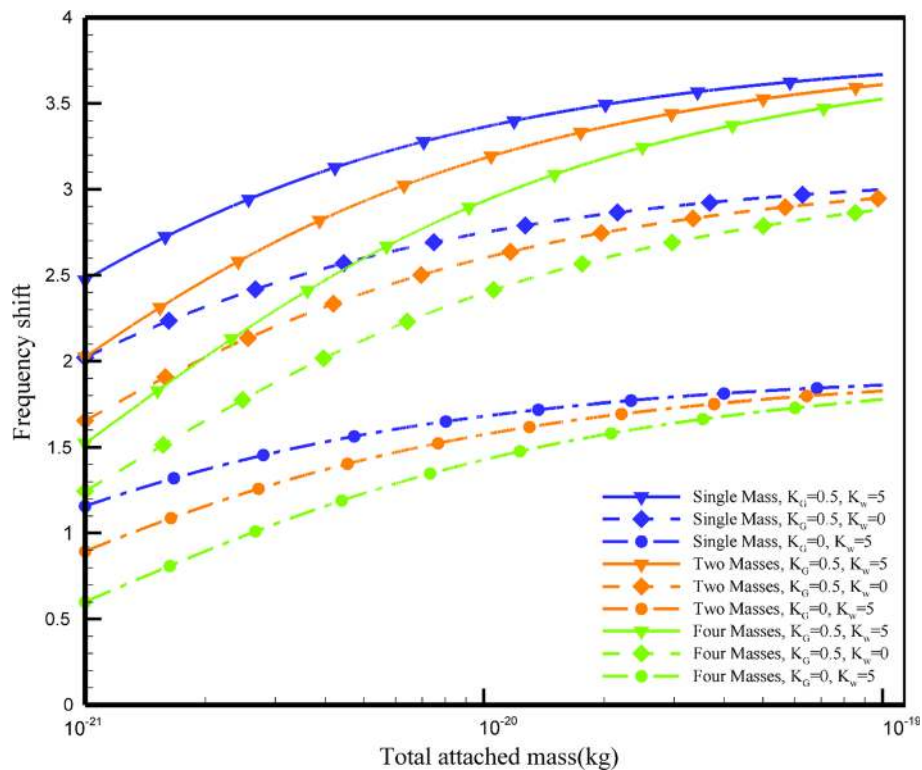
Fig. 5 The effect of Pasternak medium coefficients on the variation of the sensitivity performance of FG-MEE nanosensor (color figure online)

Fig. 6 Coupled effects of external electric voltage and number of attached nanoparticles and the total attached mass of the nanoparticles on the fundamental frequency shift (color figure online)
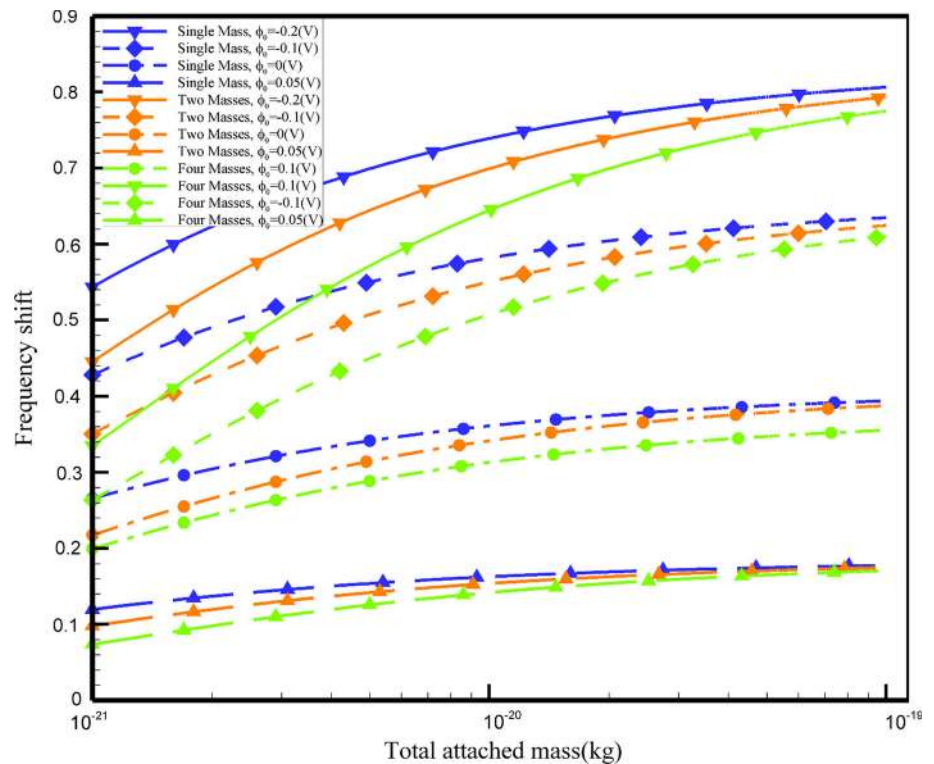
Fig. 7 Coupled effects of external magnetic potential and number of attached nanoparticles and the total attached mass of the nanoparticles on the fundamental frequency shift (color figure online)
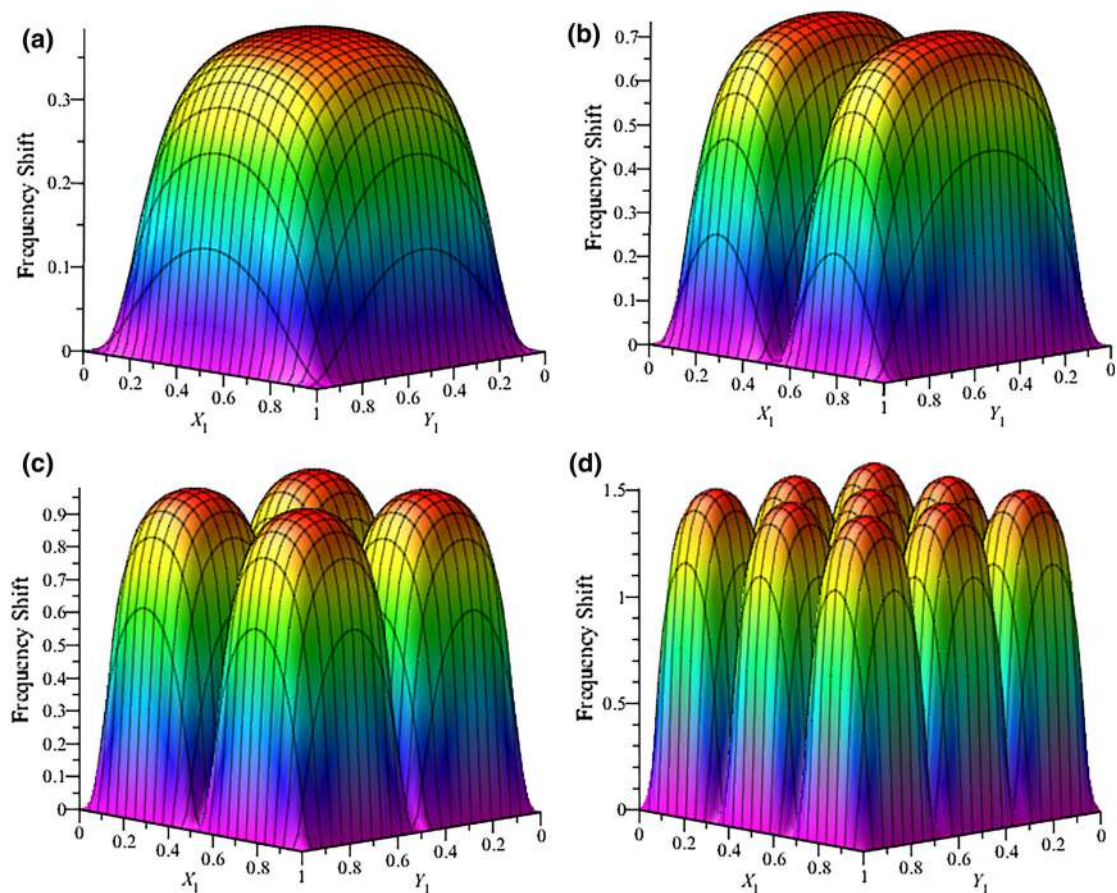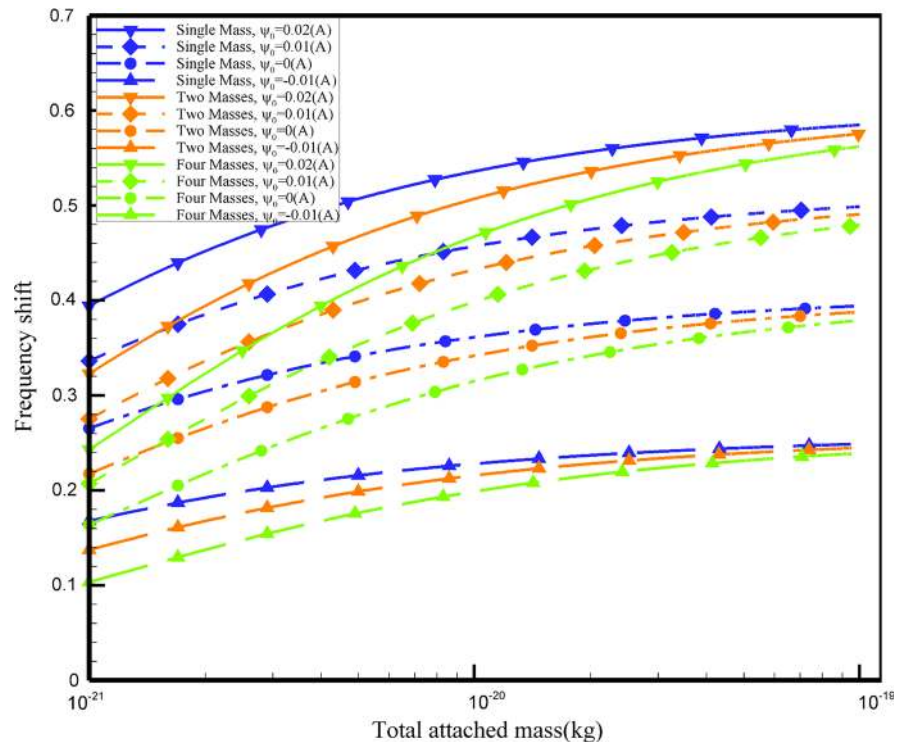

Fig. 8 The influence of attached single nanoparticle location on the sensitivity performance of FG-MEE nanosensor; (**a**) $m = n = 1$, (**b**) $m = 1, n = 2$, (**c**) $m = n = 2$, (**d**) $m = n = 3$ (color figure online)

$$\bar{C}_{11}(z) = C_{11}(z) - \frac{C_{13}(z)^2}{C_{33}(z)},$$

$$\bar{C}_{12}(z) = C_{12}(z) - \frac{C_{13}(z)C_{23}(z)}{C_{33}(z)},$$

$$\bar{C}_{22}(z) = C_{22}(z) - \frac{C_{23}(z)^2}{C_{33}(z)},$$

$$\bar{C}_{44}(z) = C_{44}(z), \ \bar{C}_{55}(z) = C_{55}(z), \ \bar{C}_{66}(z) = C_{66}(z),$$

$$\bar{e}_{31}(z) = e_{31}(z) - \frac{C_{13}(z)e_{33}(z)}{C_{33}(z)},$$

$$\bar{e}_{32}(z) = e_{32}(z) - \frac{C_{23}(z)e_{33}(z)}{C_{33}(z)},$$

$$\bar{e}_{24}(z) = e_{24}(z), \bar{e}_{15}(z) = e_{15}(z),$$

$$\bar{q}_{31}(z) = q_{31}(z) - \frac{C_{13}(z)q_{33}(z)}{C_{33}(z)},$$

$$\bar{q}_{32}(z) = q_{32}(z) - \frac{C_{23}(z)q_{33}(z)}{C_{33}(z)},$$

$$\bar{q}_{24}(z) = q_{24}(z), \ \bar{q}_{15}(z) = q_{15}(z),$$

$$\bar{\eta}_{11}(z) = \eta_{11}(z), \ \bar{\eta}_{22}(z) = \eta_{11}(z),$$

$$\bar{\eta}_{33}(z) = \eta_{33}(z) + \frac{e_{33}(z)^2}{C_{33}(z)}, \ \bar{d}_{11}(z) = d_{11}(z),$$

$$\bar{d}_{22}(z) = d_{22}(z), \ \bar{d}_{33}(z) = d_{33}(z) + \frac{q_{33}(z)e_{33}(z)}{C_{33}(z)},$$

$$\bar{\mu}_{11}(z) = \mu_{11}(z), \ \bar{\mu}_{22}(z) = \mu_{22}(z),$$

$$\bar{\mu}_{33}(z) = \mu_{33}(z) + \frac{q_{33}(z)^2}{C_{33}(z)}. \tag{8}$$

It should be noted that if the electric and magnetic fields are supposed to be the negative gradients of scalar electric $\Phi(x,y,z,t)$ and magnetic potentials $\Psi(x,y,z,t)$, respectively, Maxwell equations in the quasi-static approximation are satisfied as

$$E_i = -\frac{\partial\Phi(x,y,z,t)}{\partial i}$$
$$H_i = -\frac{\partial\Psi(x,y,z,t)}{\partial i}, (i = x,y,z) \tag{9}$$

However, in this work, the boundary conditions of magnetic and electric fields at the bottom and top surfaces of the FG-MEE nanoplate are taken to be as

$$\Phi\left(x,y,-\frac{h}{2},t\right) = -\phi_0, \Phi\left(x,y,\frac{h}{2},t\right) = \phi_0$$
$$\Psi\left(x,y,-\frac{h}{2},t\right) = -\Psi_0, \Psi\left(x,y,\frac{h}{2},t\right) = \Psi_0 \tag{10}$$

where the terms ϕ_0 and Ψ_0 ($-\phi_0$ and $-\Psi_0$) indicate, respectively, the external electric potential and magnetic potential exerting to the top (bottom) surface of FG-MEE nanoplate. With respect to the electric-magnetic boundary

conditions, the explicit distribution of electric and magnetic potentials are expressed as a combination of cosine and linear variation in the following form (Farajpour et al. 2016; Ansari and Gholami 2017)

$$\Phi(x,y,z,t) = -\cos\left(\frac{\pi z}{h}\right)\phi(x,y,t) + \frac{2z\phi_0}{h}$$
$$\Psi(x,y,z,t) = -\cos\left(\frac{\pi z}{h}\right)\psi(x,y,t) + \frac{2z\psi_0}{h} \tag{11}$$

in which $\phi(x,y,t)$ and $\psi(x,y,t)$ demonstrate the spatial variations related to the electric potential and magnetic potential along the x and y directions, respectively.

2.4 Governing equations and boundary conditions

In order to determine the governing differential equations of the motion of present model and related boundary conditions, in this section, Hamilton's principle can be applied in the below form as

$$\int_{t_1}^{t_2}(\delta T - \delta U + \delta V)dt = 0 \tag{12}$$

where $\delta T, \delta U$ and δV, respectively, denote the virtual kinetic energy, the virtual strain energy and the virtual work exerted by external force q. Here, q refers to the transverse load per unit area of FG-MEE nanoplate due to the added nanoparticle with mass m_e for eth mass in position (x_e, y_e), Pasternak elastic medium, and external loads which can be expressed as (Shen et al. 2012; Ke et al. 2014; Hosseini et al. 2016a)

$$q = -k_w w_0 + k_G\left(\frac{\partial^2 w_0}{\partial x^2} + \frac{\partial^2 w_0}{\partial y^2}\right)$$
$$- \sum_{e=1}^{p} m_e \delta(x-x_e)\delta(y-y_e)\frac{\partial^2 w_0}{\partial t^2} \tag{13}$$
$$+ (N_{Ex} + N_{Mx})\frac{\partial^2 w_0}{\partial x^2} + (N_{Ey} + N_{My})\frac{\partial^2 w_0}{\partial y^2}$$

in which $\left(N_{Ex} = \int_{-\frac{h}{2}}^{\frac{h}{2}} 2\frac{\bar{e}_{31}(z)\phi_0}{h}, N_{Ey} = \int_{-\frac{h}{2}}^{\frac{h}{2}} 2\frac{\bar{e}_{32}(z)\phi_0}{h}\right)$ and $\left(N_{Mx} = \int_{-\frac{h}{2}}^{\frac{h}{2}} 2\frac{\bar{q}_{31}(z)\psi_0}{h}, N_{My} = \int_{-\frac{h}{2}}^{\frac{h}{2}} 2\frac{\bar{q}_{32}(z)\psi_0}{h}\right)$ illustrate the normal loads induced by initial external electric potential and initial external magnetic potential along x and y coordinate directions, respectively. Also, the Dirac delta function in the two two-dimensional state is shown with symbol $\delta(x-x_e)\delta(y-y_e)$, which define as

$$\delta(x - x_e)\delta(y - y_e) = 0 \quad for(x, y) \neq (x_e, y_e)$$

$$\int\limits_{-\infty}^{\infty} \int\limits_{-\infty}^{\infty} \delta(x - x_e)\delta(y - y_e)dxdy = 1. \tag{14}$$

2.4.1 Virtual kinetic energy

The virtual kinetic energy on the basis of the first shear order deformation theory can be written as follows

$$\delta T = \int \left[I_0(\dot{u}_0 \delta\dot{u}_0 + \dot{v}_0 \delta\dot{v}_0 + \dot{w}_0 \delta\dot{w}_0) \right.$$
$$+ I_1\left(\dot{u}_0 \delta\dot{\theta}_x + \dot{\theta}_x \delta\dot{u}_0 + \dot{v}_0 \delta\dot{\theta}_y + \dot{\theta}_y \delta\dot{v}_0\right)$$
$$\left. + I_2\left(\dot{\theta}_x \delta\dot{\theta}_x + \dot{\theta}_y \delta\dot{\theta}_y\right) \right] dA \tag{15}$$

where I_0, I_1 and I_2 denote the mass inertia terms which can be expressed as $\{I_0, I_1, I_2\} = \int_{-\frac{h}{2}}^{\frac{h}{2}} \{\rho(z), \rho(z)z, \rho(z)z^2\}dz.$

2.4.2 Virtual strain energy

The variation of strain energy using the first shear order deformation theory can be expressed as

$$\delta U = \int \left[N_{xx}\frac{\partial\delta u_0}{\partial x} + N_{yy}\frac{\partial\delta v_0}{\partial y} + M_{xx}\frac{\partial\delta\theta_x}{\partial x} + M_{yy}\frac{\partial\delta\theta_y}{\partial y} \right.$$
$$+ N_{xy}\left(\frac{\partial\delta u_0}{\partial y} + \frac{\partial\delta v_0}{\partial x}\right) + M_{xy}\left(\frac{\partial\delta\theta_x}{\partial y} + \frac{\partial\delta\theta_y}{\partial x}\right)$$
$$\left. + Q_{xx}\left(\delta\theta_x + \frac{\partial\delta w_0}{\partial x}\right) + Q_{yy}\left(\delta\theta_y + \frac{\partial\delta w_0}{\partial y}\right) \right] dA$$
$$- \int\int\limits_{-\frac{h}{2}}^{\frac{h}{2}} (D_x\delta E_x + D_y\delta E_y + D_z\delta E_z + B_x\delta H_x + B_y\delta H_y$$
$$+ B_z\delta H_z)dzdA \tag{16}$$

in which parameters N_{ij}, M_{ij} and Q_{ii} can be defined by the following integral expressions

$$\{N_{xx}, N_{yy}, N_{xy}\} = \int\limits_{-\frac{h}{2}}^{\frac{h}{2}} \{\sigma_{xx}, \sigma_{yy}, \sigma_{xy}\}dz, \{M_{xx}, M_{yy}, M_{xy}\}$$

$$= \int\limits_{-\frac{h}{2}}^{\frac{h}{2}} \{\sigma_{xx}, \sigma_{yy}, \sigma_{xy}\}zdz, \{Q_{xx}, Q_{yy}\}$$

$$= k_s \int\limits_{-\frac{h}{2}}^{\frac{h}{2}} \{\sigma_{xz}, \sigma_{yz}\}dz. \tag{17}$$

The term k_s is the shear correction factor and here equals to 5/6.

2.4.3 Virtual work

Variation of work applied by external loads denotes by

$$\delta V = \int q\delta w_0 dA \tag{18}$$

2.4.4 The equilibrium equations in terms of the displacements

Finally, by implementing relations (15–18) into Hamilton's variational principle and integrating by parts, and factoring the coefficients of $\delta u_0, \delta v_0, \delta w_0, \delta\theta_x, \delta\theta_y, \delta\phi$ and $\delta\psi$, the following equilibrium equations of motion are derived as

$$\delta u_0 : \frac{\partial N_{xx}}{\partial x} + \frac{\partial N_{xy}}{\partial y} = I_0\frac{\partial^2 u_0}{\partial t^2} + I_1\frac{\partial^2\theta_x}{\partial t^2} \tag{19-1}$$

$$\delta v_0 : \frac{\partial N_{xy}}{\partial x} + \frac{\partial N_{yy}}{\partial y} = I_0\frac{\partial^2 v_0}{\partial t^2} + I_1\frac{\partial^2\theta_y}{\partial t^2} \tag{19-2}$$

$$\delta w_0 : \frac{\partial Q_{xx}}{\partial x} + \frac{\partial Q_{yy}}{\partial y} + q = I_0\frac{\partial^2 w_0}{\partial t^2} \tag{19-3}$$

$$\delta\theta_x : \frac{\partial M_{xx}}{\partial x} + \frac{\partial M_{xy}}{\partial y} - Q_{xx} = I_1\frac{\partial^2 u_0}{\partial t^2} + I_2\frac{\partial^2\theta_x}{\partial t^2} \tag{19-4}$$

$$\delta\theta_y : \frac{\partial M_{yy}}{\partial y} + \frac{\partial M_{xy}}{\partial x} - Q_{yy} = I_1\frac{\partial^2 v_0}{\partial t^2} + I_2\frac{\partial^2\theta_y}{\partial t^2} \tag{19-5}$$

$$\delta\phi : \int\limits_{-\frac{h}{2}}^{\frac{h}{2}} \left(\frac{\partial D_x}{\partial x}\cos\left(\frac{\pi z}{h}\right) + \frac{\partial D_y}{\partial y}\cos\left(\frac{\pi z}{h}\right) + \frac{\pi}{h}D_z\sin\left(\frac{\pi z}{h}\right) \right)dz$$
$$= 0 \tag{19-6}$$

$$\delta\psi : \int_{-\frac{h}{2}}^{\frac{h}{2}} \left(\frac{\partial B_x}{\partial x}\cos\left(\frac{\pi z}{h}\right) + \frac{\partial B_y}{\partial y}\cos\left(\frac{\pi z}{h}\right) + \frac{\pi}{h}B_z\sin\left(\frac{\pi z}{h}\right) \right) dz$$
$$= 0$$
$$(19-7)$$

and the related natural and necessary boundary conditions with normal vectors n_x and n_y are obtained along borders x and y as below

$$\delta u_0 = 0 \quad \text{or} \quad N_{xx}n_x + N_{xy}n_y = 0 \qquad (20-1)$$

$$\delta v_0 = 0 \quad \text{or} \quad N_{xy}n_x + N_{yy}n_y = 0 \qquad (20-2)$$

$$\delta w_0 = 0 \quad \text{or} \quad \left(Q_{xx} + k_G\frac{\partial w}{\partial x}\right)n_x + \left(Q_{yy} + k_G\frac{\partial w}{\partial y}\right)n_y = 0$$
$$(20-3)$$

$$\delta\theta_x = 0 \quad \text{or} \quad M_{xx}n_x + M_{xy}n_y = 0 \qquad (20-4)$$

$$\delta\theta_y = 0 \quad \text{or} \quad M_{xy}n_x + M_{yy}n_y = 0 \qquad (20-5)$$

$$\delta\phi = 0 \quad \text{or} \quad \int_{-\frac{h}{2}}^{\frac{h}{2}} \left[n_x D_x\cos\left(\frac{\pi z}{h}\right) + n_y D_y\cos\left(\frac{\pi z}{h}\right) \right] dz = 0$$
$$(20-6)$$

$$\delta\psi = 0 \quad \text{or} \quad \int_{-\frac{h}{2}}^{\frac{h}{2}} \left[n_x B_x\cos\left(\frac{\pi z}{h}\right) + n_y B_y\cos\left(\frac{\pi z}{h}\right) \right] dz = 0$$
$$(20-7)$$

The following nonlocal expressions in terms of displacements can be written by integrating Eq. (6) over the area of nanoplate cross-section

$$\left[1 - (e_0 a)^2\nabla^2\right]N_{xx} = A_{11}\frac{\partial u_0}{\partial x} + A_{12}\frac{\partial v_0}{\partial y} + B_{11}\frac{\partial\theta_x}{\partial x}$$
$$+ B_{12}\frac{\partial\theta_y}{\partial y} + E_{11}\phi + F_{11}\psi + N_{xx1}^E$$
$$+ N_{xx1}^M$$
$$(21-1)$$

$$\left[1 - (e_0 a)^2\nabla^2\right]N_{yy} = A_{12}\frac{\partial u_0}{\partial x} + A_{22}\frac{\partial v_0}{\partial y} + B_{12}\frac{\partial\theta_x}{\partial x}$$
$$+ B_{22}\frac{\partial\theta_y}{\partial y} + G_{11}\phi + H_{11}\psi + N_{yy1}^E$$
$$+ N_{yy1}^M$$
$$(21-2)$$

$$\left[1 - (e_0 a)^2\nabla^2\right]N_{xy} = A_{66}\left(\frac{\partial u_0}{\partial y} + \frac{\partial v_0}{\partial x}\right) + B_{66}\left(\frac{\partial\theta_x}{\partial y} + \frac{\partial\theta_y}{\partial x}\right)$$
$$(21-3)$$

$$\left[1 - (e_0 a)^2\nabla^2\right]M_{xx} = B_{11}\frac{\partial u_0}{\partial x} + B_{12}\frac{\partial v_0}{\partial y} + D_{11}\frac{\partial\theta_x}{\partial x}$$
$$+ D_{12}\frac{\partial\theta_y}{\partial y} + E_{22}\phi + F_{22}\psi + N_{xx2}^E$$
$$+ N_{xx2}^M$$
$$(21-4)$$

$$\left[1 - (e_0 a)^2\nabla^2\right]M_{yy} = B_{12}\frac{\partial u_0}{\partial x} + B_{22}\frac{\partial v_0}{\partial y} + D_{12}\frac{\partial\theta_x}{\partial x}$$
$$+ D_{22}\frac{\partial\theta_y}{\partial y} + G_{22}\phi + H_{22}\psi + N_{yy2}^E$$
$$+ N_{yy2}^M$$
$$(21-5)$$

$$\left[1 - (e_0 a)^2\nabla^2\right]M_{xy} = B_{66}\left(\frac{\partial u_0}{\partial y} + \frac{\partial v_0}{\partial x}\right)$$
$$+ D_{66}\left(\frac{\partial\theta_x}{\partial y} + \frac{\partial\theta_y}{\partial x}\right) \qquad (21-6)$$

$$\left[1-(e_0a)^2\nabla^2\right]Q_{xx}=k_sA_{55}\left(\theta_x+\frac{\partial w_0}{\partial x}\right)-k_sJ_2\frac{\partial\phi}{\partial x}$$
$$-k_sJ_3\frac{\partial\psi}{\partial x}$$

$$(21-7)$$

$$\left[1-(e_0a)^2\nabla^2\right]Q_{yy}=k_sA_{44}\left(\theta_y+\frac{\partial w_0}{\partial y}\right)-k_sL_2\frac{\partial\phi}{\partial y}$$
$$-k_sL_3\frac{\partial\psi}{\partial y}$$

$$(21-8)$$

$$\int_{-\frac{h}{2}}^{\frac{h}{2}}\left[1-(e_0a)^2\nabla^2\right]D_x\cos\left(\frac{\pi z}{h}\right)$$
$$=J_2\left(\theta_x+\frac{\partial w_0}{\partial x}\right)+Q_1\frac{\partial\phi}{\partial x}+Q_2\frac{\partial\psi}{\partial x}$$

$$(21-9)$$

$$\int_{-\frac{h}{2}}^{\frac{h}{2}}\left[1-(e_0a)^2\nabla^2\right]D_y\cos\left(\frac{\pi z}{h}\right)$$
$$=L_2\left(\theta_y+\frac{\partial w_0}{\partial y}\right)+X_1\frac{\partial\phi}{\partial y}+X_2\frac{\partial\psi}{\partial y}$$

$$(21-10)$$

$$\int_{-\frac{h}{2}}^{\frac{h}{2}}\left[1-(e_0a)^2\nabla^2\right]D_z\left(\frac{\pi}{h}\right)\sin\left(\frac{\pi z}{h}\right)$$
$$=E_{11}\frac{\partial u_0}{\partial x}+G_{11}\frac{\partial v_0}{\partial y}+E_{22}\frac{\partial\theta_x}{\partial x}+G_{22}\frac{\partial\theta_y}{\partial y}-P_1\phi-P_2\psi$$
$$-N_{xx3}^E+N_{xx3}^M$$

$$(21-11)$$

$$\int_{-\frac{h}{2}}^{\frac{h}{2}}\left[1-(e_0a)^2\nabla^2\right]B_x\cos\left(\frac{\pi z}{h}\right)$$
$$=J_3\left(\theta_x+\frac{\partial w_0}{\partial x}\right)+Q_2\frac{\partial\phi}{\partial x}+Q_3\frac{\partial\psi}{\partial x}$$

$$(21-12)$$

$$\int_{-\frac{h}{2}}^{\frac{h}{2}}\left[1-(e_0a)^2\nabla^2\right]B_y\cos\left(\frac{\pi z}{h}\right)$$
$$=L_3\left(\theta_y+\frac{\partial w_0}{\partial y}\right)+X_2\frac{\partial\phi}{\partial y}+X_3\frac{\partial\psi}{\partial y}$$

$$(21-13)$$

$$\int_{-\frac{h}{2}}^{\frac{h}{2}}\left[1-(e_0a)^2\nabla^2\right]B_z\left(\frac{\pi}{h}\right)\sin\left(\frac{\pi z}{h}\right)$$
$$=F_{11}\frac{\partial u_0}{\partial x}+H_{11}\frac{\partial v_0}{\partial y}+F_{22}\frac{\partial\theta_x}{\partial x}+H_{22}\frac{\partial\theta_y}{\partial y}-P_2\phi-P_3\psi$$
$$-N_{yy3}^E+N_{yy3}^M$$

$$(21-14)$$

where parameters $N_{xxi}^E, N_{xxi}^M, N_{yyi}^E, N_{yyi}^M, A_{ij}, B_{ij}, D_{ij}, E_{ij}, F_{ij},$ $G_{ij}, H_{ij}, J_i, L_i, Q_i, X_i$ and P_i are represented in integral forms, which are provided in appendix A. By substituting Eqs. (21-1–21-14) into (19-1–19-7), the neoclassical governing equations of FG-METE Mindlin nanoplate in terms of displacements can be obtained as:

$$\delta u_0 : A_{11}\frac{\partial^2 u_0}{\partial x^2}+A_{12}\frac{\partial^2 v_0}{\partial x\partial y}+B_{13}\frac{\partial^2\theta_x}{\partial x^2}+B_{12}\frac{\partial^2\theta_y}{\partial x\partial y}$$
$$+E_{11}\frac{\partial\phi}{\partial x}+F_{11}\frac{\partial\psi}{\partial x}$$
$$+A_{66}\left(\frac{\partial^2 u_0}{\partial y^2}+\frac{\partial^2 v_0}{\partial x\partial y}\right)+B_{66}\left(\frac{\partial^2\theta_x}{\partial y^2}+\frac{\partial^2\theta_y}{\partial x\partial y}\right)$$
$$=\left[1-(e_0a)^2\nabla^2\right]\left(I_0\frac{\partial^2 u_0}{\partial t^2}+I_1\frac{\partial^2\theta_x}{\partial t^2}\right)$$

$$(22)$$

$$\delta v_0 : A_{66}\left(\frac{\partial^2 v_0}{\partial x^2}+\frac{\partial^2 u_0}{\partial x\partial y}\right)+B_{66}\left(\frac{\partial^2\theta_x}{\partial x\partial y}+\frac{\partial^2\theta_y}{\partial x^2}\right)$$
$$+A_{12}\frac{\partial^2 u_0}{\partial x\partial y}+A_{22}\frac{\partial^2 v_0}{\partial y^2}+B_{12}\frac{\partial^2\theta_x}{\partial x\partial y}$$
$$+B_{22}\frac{\partial^2\theta_y}{\partial y^2}+G_{11}\frac{\partial\phi}{\partial y}+H_{11}\frac{\partial\psi}{\partial y}$$
$$=\left[1-(e_0a)^2\nabla^2\right]\left(I_0\frac{\partial^2 v_0}{\partial t^2}+I_1\frac{\partial^2\theta_y}{\partial t^2}\right)$$

$$(23)$$

$$\delta w_0 : k_sA_{55}\left(\frac{\partial\theta_x}{\partial x}+\frac{\partial^2 w_0}{\partial x^2}\right)+k_sA_{44}\left(\frac{\partial\theta_y}{\partial y}+\frac{\partial^2 w_0}{\partial y^2}\right)$$
$$-k_sJ_2\frac{\partial^2\phi}{\partial x^2}-k_sJ_3\frac{\partial^2\psi}{\partial x^2}-k_sL_2\frac{\partial^2\phi}{\partial y^2}-k_sL_3\frac{\partial^2\psi}{\partial y^2}$$
$$+\left[1-(e_0a)^2\nabla^2\right]$$
$$\left[(N_{Ex}+N_{Mx})\frac{\partial^2 w_0}{\partial x^2}+(N_{Ey}+N_{My})\frac{\partial^2 w_0}{\partial y^2}-k_ww_0\right.$$
$$\left.+k_G\left(\frac{\partial^2 w_0}{\partial x^2}+\frac{\partial^2 w_0}{\partial y^2}\right)\right]$$
$$=\left[1-(e_0a)^2\nabla^2\right]\left[\left(I_0+\sum_{e=1}^{p}m_e\delta(x-x_e)\delta(y-y_e)\right)\frac{\partial^2 w_0}{\partial t^2}\right]$$

$$(24)$$

$$\delta\theta_x : B_{11}\frac{\partial^2 u_0}{\partial x^2}+B_{12}\frac{\partial^2 v_0}{\partial x\partial y}+D_{11}\frac{\partial^2\theta_x}{\partial x^2}+D_{12}\frac{\partial^2\theta_y}{\partial x\partial y}$$
$$+(E_{22}+k_sJ_2)\frac{\partial\phi}{\partial x}+(F_{22}+k_sJ_3)\frac{\partial\psi}{\partial x}+B_{66}\left(\frac{\partial^2 u_0}{\partial y^2}+\frac{\partial^2 v_0}{\partial x\partial y}\right)$$
$$+D_{66}\left(\frac{\partial^2\theta_x}{\partial y^2}+\frac{\partial^2\theta_y}{\partial x\partial y}\right)-k_sA_{55}\left(\theta_x+\frac{\partial w_0}{\partial x}\right)$$
$$=\left[1-(e_0a)^2\nabla^2\right]\left(I_1\frac{\partial^2 u_0}{\partial t^2}+I_2\frac{\partial^2\theta_x}{\partial t^2}\right)$$

$$(25)$$

$$\delta\theta_y : B_{12}\frac{\partial^2 u_0}{\partial x \partial y} + B_{22}\frac{\partial^2 v_0}{\partial y^2} + D_{12}\frac{\partial^2 \theta_x}{\partial x \partial y} + D_{22}\frac{\partial^2 \theta_y}{\partial y^2}$$

$$+ (G_{22} + k_s L_2)\frac{\partial \phi}{\partial y}$$

$$+ (H_{22} + k_s L_3)\frac{\partial \psi}{\partial y} + B_{66}\left(\frac{\partial^2 u_0}{\partial x \partial y} + \frac{\partial^2 v_0}{\partial x^2}\right)$$

$$+ D_{66}\left(\frac{\partial^2 \theta_x}{\partial x \partial y} + \frac{\partial^2 \theta_y}{\partial x^2}\right) - k_s A_{44}\left(\theta_y + \frac{\partial w_0}{\partial y}\right)$$

$$= \left[1 - (e_0 a)^2 \nabla^2\right]\left(I_1\frac{\partial^2 v_0}{\partial t^2} + I_2\frac{\partial^2 \theta_y}{\partial t^2}\right) \tag{26}$$

$$\delta\phi : J_2\left(\frac{\partial \theta_x}{\partial x} + \frac{\partial^2 w_0}{\partial x^2}\right) + L_2\left(\frac{\partial \theta_y}{\partial y} + \frac{\partial^2 w_0}{\partial y^2}\right) + Q_1\frac{\partial^2 \phi}{\partial x^2}$$

$$+ Q_2\frac{\partial^2 \psi}{\partial x^2}$$

$$+ X_1\frac{\partial^2 \phi}{\partial y^2} + X_2\frac{\partial^2 \psi}{\partial y^2} + E_{11}\frac{\partial u_0}{\partial x} + G_{11}\frac{\partial v_0}{\partial y} + E_{22}\frac{\partial \theta_x}{\partial x}$$

$$+ G_{22}\frac{\partial \theta_y}{\partial y} - P_1\phi - P_2\psi = 0 \tag{27}$$

$$\delta\psi : J_3\left(\frac{\partial \theta_x}{\partial x} + \frac{\partial^2 w_0}{\partial x^2}\right) + L_3\left(\frac{\partial \theta_y}{\partial y} + \frac{\partial^2 w_0}{\partial y^2}\right) + Q_2\frac{\partial^2 \phi}{\partial x^2}$$

$$+ Q_3\frac{\partial^2 \psi}{\partial x^2}$$

$$+ X_2\frac{\partial^2 \phi}{\partial y^2} + X_3\frac{\partial^2 \psi}{\partial y^2} + F_{11}\frac{\partial u_0}{\partial x} + H_{11}\frac{\partial v_0}{\partial y} + F_{22}\frac{\partial \theta_x}{\partial x}$$

$$+ H_{22}\frac{\partial \theta_y}{\partial y} - P_2\phi - P_3\psi = 0 \tag{28}$$

2.5 Dimensionless expressions of equilibrium equations

By suggesting the following non-dimensional phrases, the linear equations (22–28) can be rewritten in a non-dimensional form

$$X = \frac{x}{l_x}, \quad Y = \frac{y}{l_y}, \quad \bar{w} = \frac{w_0}{h}, \quad \bar{\phi} = \frac{\phi}{\bar{\phi}_0}, \quad \bar{\psi} = \frac{\psi}{\bar{\psi}_0},$$

$$\bar{u} = \frac{u_0}{h}, \quad \bar{v} = \frac{v_0}{h}, \quad \bar{\phi}_0 = \sqrt{\frac{A_{11}^0}{P_1}},$$

$$\bar{\psi}_0 = \sqrt{\frac{A_{11}^0}{P_3}}, \quad r = \frac{l_x}{h}, \quad R = \frac{l_x}{l_y}, \quad \tau^2 = \frac{t^2 A_{11}^0}{l_x^2 I_0^0}, \quad \bar{K}_w = \frac{k_w l_x^2}{A_{11}^0},$$

$$\bar{K}_G = \frac{k_G}{A_{11}^0}, \quad \mu = \frac{e_0 a}{l_x} \tag{29}$$

where $A_{11}^0 = (\bar{C}_{11})_{\text{BaTiO}_3} h$ and $I_0^0 = (\rho)_{\text{BaTiO}_3} h$. After applying the above dimensionless phrases into Eqs. (22–28), the non-dimensional form of the constitutive equations of FG-MEE nanoplate can be introduced as

$$\delta\bar{u} : \bar{A}_{11}\frac{\partial^2 \bar{u}}{\partial X^2} + \bar{A}_{12}R\frac{\partial^2 \bar{v}}{\partial X \partial Y} + \bar{B}_{11}\frac{\partial^2 \theta_x}{\partial X^2} + \bar{B}_{12}R\frac{\partial^2 \theta_y}{\partial X \partial Y}$$

$$+ \bar{E}_{11}r\frac{\partial \bar{\phi}}{\partial X} + \bar{F}_{11}r\frac{\partial \bar{\psi}}{\partial X} + \bar{A}_{66}\left(R^2\frac{\partial^2 \bar{u}}{\partial Y^2} + R\frac{\partial^2 \bar{v}}{\partial X \partial Y}\right)$$

$$+ \bar{B}_{66}\left(R^2\frac{\partial^2 \theta_x}{\partial Y^2} + R\frac{\partial^2 \theta_y}{\partial X \partial Y}\right) = \left[1 - \mu^2\left(\frac{\partial^2}{\partial X^2} + R^2\frac{\partial^2}{\partial Y^2}\right)\right]$$

$$\left(\frac{I_0}{I_0^0}\frac{\partial^2 \bar{u}}{\partial \tau^2} + \frac{I_1}{I_0^0 h}\frac{\partial^2 \theta_x}{\partial \tau^2}\right) \tag{30}$$

$$\delta\bar{v} : \bar{A}_{66}\left(\frac{\partial^2 \bar{v}}{\partial X^2} + R\frac{\partial^2 \bar{u}}{\partial X \partial Y}\right) + \bar{B}_{66}\left(R\frac{\partial^2 \theta_x}{\partial X \partial Y} + \frac{\partial^2 \theta_y}{\partial X^2}\right)$$

$$+ \bar{A}_{12}R\frac{\partial^2 \bar{u}}{\partial X \partial Y} + \bar{A}_{22}R^2\frac{\partial^2 \bar{v}}{\partial Y^2}$$

$$+ \bar{B}_{12}R\frac{\partial^2 \theta_x}{\partial X \partial Y} + \bar{B}_{22}R^2\frac{\partial^2 \theta_y}{\partial Y^2} + \bar{G}_{11}Rr\frac{\partial \bar{\phi}}{\partial Y}$$

$$+ \bar{H}_{11}Rr\frac{\partial \bar{\psi}}{\partial Y} = \left[1 - \mu^2\left(\frac{\partial^2}{\partial X^2} + R^2\frac{\partial^2}{\partial Y^2}\right)\right]$$

$$\left(\frac{I_0}{I_0^0}\frac{\partial^2 \bar{v}}{\partial \tau^2} + \frac{I_1}{I_0^0 h}\frac{\partial^2 \theta_y}{\partial \tau^2}\right) \tag{31}$$

$$\delta\bar{w} : k_s\bar{A}_{55}\left(\frac{\partial \theta_x}{\partial X} + \frac{1}{r}\frac{\partial^2 \bar{w}}{\partial X^2}\right) + k_s\bar{A}_{44}\left(R\frac{\partial \theta_y}{\partial Y} + \frac{R^2}{r}\frac{\partial^2 \bar{w}}{\partial Y^2}\right)$$

$$- k_s\frac{\bar{J}_2}{r}\frac{\partial^2 \bar{\phi}}{\partial X^2} - k_s\frac{\bar{J}_3}{r}\frac{\partial^2 \bar{\psi}}{\partial X^2}$$

$$- k_s\frac{\bar{L}_2 R^2}{r}\frac{\partial^2 \bar{\phi}}{\partial Y^2} - k_s\frac{\bar{L}_3 R^2}{r}\frac{\partial^2 \bar{\psi}}{\partial Y^2} + \frac{1}{r}$$

$$\left[1 - \mu^2\left(\frac{\partial^2}{\partial X^2} + R^2\frac{\partial^2}{\partial Y^2}\right)\right]$$

$$\left[\frac{(N_{Ex} + N_{Mx})}{A_{11}^0}\frac{\partial^2 \bar{w}}{\partial X^2} + \frac{(N_{Ey} + N_{My})R^2}{A_{11}^0}\frac{\partial^2 w_0}{\partial y^2}\right.$$

$$\left. - \bar{K}_w\bar{w} + \bar{K}_G\left(\frac{\partial^2 \bar{w}}{\partial X^2} + R^2\frac{\partial^2 \bar{w}}{\partial Y^2}\right)\right]$$

$$= \frac{1}{r}\left[1 - \mu^2\left(\frac{\partial^2}{\partial X^2} + R^2\frac{\partial^2}{\partial Y^2}\right)\right]$$

$$\left[\left(\frac{I_0}{I_0^0} + \sum_{e=1}^{p}\frac{m_e}{I_0^0 l_x l_y}\delta(X - X_e)\delta(Y - Y_e)\right)\frac{\partial^2 \bar{w}}{\partial \tau^2}\right] \tag{32}$$

$$\delta\theta_x : \bar{B}_{11}\frac{\partial^2\bar{u}}{\partial X^2} + \bar{B}_{12}R\frac{\partial^2\bar{v}}{\partial X\partial Y} + \bar{D}_{11}\frac{\partial^2\theta_x}{\partial X^2} + \bar{D}_{12}R\frac{\partial^2\theta_y}{\partial X\partial Y}$$

$$+ (\bar{E}_{22} + k_s\bar{J}_2)r\frac{\partial\bar{\phi}}{\partial X}$$

$$+ (\bar{F}_{22} + k_s\bar{J}_3)r\frac{\partial\bar{\psi}}{\partial X} + \bar{B}_{66}\left(R^2\frac{\partial^2\bar{u}}{\partial Y^2} + R\frac{\partial^2\bar{v}}{\partial X\partial Y}\right)$$

$$+ \bar{D}_{66}\left(R^2\frac{\partial^2\theta_x}{\partial Y^2} + R\frac{\partial^2\theta_y}{\partial X\partial Y}\right)$$

$$- k_s\bar{A}_{55}\left(r^2\theta_x + r\frac{\partial\bar{w}}{\partial X}\right) = \left[1 - \mu^2\left(\frac{\partial^2}{\partial X^2} + R^2\frac{\partial^2}{\partial Y^2}\right)\right]$$

$$\left(\frac{I_1}{I_0^0 h}\frac{\partial^2\bar{v}}{\partial\tau^2} + \frac{I_2}{I_0^0 h^2}\frac{\partial^2\theta_x}{\partial\tau^2}\right)$$

$$\tag{33}$$

$$\delta\theta_y : \bar{B}_{12}R\frac{\partial^2\bar{u}}{\partial X\partial Y} + \bar{B}_{22}R^2\frac{\partial^2\bar{v}}{\partial Y^2} + \bar{D}_{12}R\frac{\partial^2\theta_x}{\partial X\partial Y}$$

$$+ \bar{D}_{22}R^2\frac{\partial^2\theta_y}{\partial Y^2} + (\bar{G}_{22} + k_s\bar{L}_2)Rr\frac{\partial\bar{\phi}}{\partial Y} + (\bar{H}_{22} + k_s\bar{L}_3)$$

$$Rr\frac{\partial\bar{\psi}}{\partial Y} + \bar{B}_{66}\left(R\frac{\partial^2\bar{u}}{\partial X\partial Y} + \frac{\partial^2\bar{v}}{\partial X^2}\right)$$

$$+ \bar{D}_{66}\left(R\frac{\partial^2\theta_x}{\partial X\partial Y} + \frac{\partial^2\theta_y}{\partial X^2}\right) - k_s\bar{A}_{44}\left(r^2\theta_y + rR\frac{\partial\bar{w}}{\partial Y}\right)$$

$$= \left[1 - \mu^2\left(\frac{\partial^2}{\partial X^2} + R^2\frac{\partial^2}{\partial Y^2}\right)\right]\left(\frac{I_1}{I_0^0 h}\frac{\partial^2\bar{v}}{\partial\tau^2} + \frac{I_2}{I_0^0 h^2}\frac{\partial^2\theta_y}{\partial\tau^2}\right)$$

$$\tag{34}$$

$$\delta\bar{\phi} : \bar{J}_2\left(\frac{\partial\theta_x}{\partial X} + \frac{1}{r}\frac{\partial^2\bar{w}}{\partial X^2}\right) + \bar{L}_2\left(R\frac{\partial\theta_y}{\partial Y} + \frac{R^2}{r}\frac{\partial^2\bar{w}}{\partial Y^2}\right)$$

$$+ \frac{1}{r}\bar{Q}_1\frac{\partial^2\bar{\phi}}{\partial X^2} + \frac{1}{r}\bar{Q}_2\frac{\partial^2\bar{\psi}}{\partial X^2}$$

$$+ \frac{R^2}{r}\bar{X}_1\frac{\partial^2\bar{\phi}}{\partial Y^2} + \frac{R^2}{r}\bar{X}_2\frac{\partial^2\bar{\psi}}{\partial Y^2} + \bar{E}_{11}\frac{\partial\bar{u}}{\partial X}$$

$$+ \bar{G}_{11}R\frac{\partial\bar{v}}{\partial Y} + \bar{E}_{22}\frac{\partial\theta_x}{\partial X} + \bar{G}_{22}R\frac{\partial\theta_y}{\partial Y} - \bar{P}_1 r\bar{\phi} - \bar{P}_2 r\bar{\psi} = 0$$

$$\tag{35}$$

$$\delta\bar{\psi} : \bar{J}_3\left(\frac{\partial\theta_x}{\partial X} + \frac{1}{r}\frac{\partial^2\bar{w}}{\partial X^2}\right) + \bar{L}_3\left(R\frac{\partial\theta_y}{\partial Y} + \frac{R^2}{r}\frac{\partial^2\bar{w}}{\partial Y^2}\right)$$

$$+ \frac{1}{r}\bar{Q}_2\frac{\partial^2\bar{\phi}}{\partial X^2}$$

$$+ \frac{1}{r}\bar{Q}_3\frac{\partial^2\bar{\psi}}{\partial X^2} + \frac{R^2}{r}\bar{X}_2\frac{\partial^2\bar{\phi}}{\partial Y^2} + \frac{R^2}{r}\bar{X}_3\frac{\partial^2\bar{\psi}}{\partial Y^2}$$

$$+ \bar{F}_{11}\frac{\partial\bar{u}}{\partial X} + \bar{H}_{11}R\frac{\partial\bar{v}}{\partial Y} + \bar{F}_{22}\frac{\partial\theta_x}{\partial X} + \bar{H}_{22}R\frac{\partial\theta_y}{\partial Y}$$

$$- \bar{P}_2 r\bar{\phi} - \bar{P}_3 r\bar{\psi} = 0$$

$$\tag{36}$$

in which

$$\{\bar{A}_{11}, \bar{A}_{12}, \bar{A}_{22}, \bar{A}_{44}, \bar{A}_{55}, \bar{A}_{66}\} = \left\{\frac{A_{11}}{A_{11}^0}, \frac{A_{12}}{A_{11}^0}, \frac{A_{22}}{A_{11}^0}, \frac{A_{44}}{A_{11}^0}, \frac{A_{55}}{A_{11}^0}, \frac{A_{66}}{A_{11}^0}\right\},$$

$$\{\bar{B}_{11}, \bar{B}_{12}, \bar{B}_{22}, \bar{B}_{66}\} = \left\{\frac{B_{11}}{A_{11}^0 h}, \frac{B_{12}}{A_{11}^0 h}, \frac{B_{22}}{A_{11}^0 h}, \frac{B_{66}}{A_{11}^0 h}\right\},$$

$$\{\bar{D}_{11}, \bar{D}_{12}, \bar{D}_{22}, \bar{D}_{66}\} = \left\{\frac{D_{11}}{A_{11}^0 h^2}, \frac{D_{12}}{A_{11}^0 h^2}, \frac{D_{22}}{A_{11}^0 h^2}, \frac{D_{66}}{A_{11}^0 h^2}\right\},$$

$$\{\bar{E}_{11}, \bar{E}_{22}\} = \left\{\frac{E_{11}\bar{\phi}_0}{A_{11}^0}, \frac{E_{22}\bar{\phi}_0}{A_{11}^0 h}\right\},$$

$$\{\bar{F}_{11}, \bar{F}_{22}\} = \left\{\frac{F_{11}\bar{\psi}_0}{A_{11}^0}, \frac{F_{22}\bar{\psi}_0}{A_{11}^0 h}\right\},$$

$$\{\bar{G}_{11}, \bar{G}_{22}\} = \left\{\frac{G_{11}\bar{\phi}_0}{A_{11}^0}, \frac{G_{22}\bar{\phi}_0}{A_{11}^0 h}\right\},$$

$$\{\bar{H}_{11}, \bar{H}_{22}\} = \left\{\frac{H_{11}\bar{\psi}_0}{A_{11}^0}, \frac{H_{22}\bar{\psi}_0}{A_{11}^0 h}\right\},$$

$$\{\bar{J}_2, \bar{J}_3\} = \left\{\frac{J_2\bar{\phi}_0}{A_{11}^0 h}, \frac{J_3\bar{\psi}_0}{A_{11}^0 h}\right\},$$

$$\{\bar{L}_2, \bar{L}_3\} = \left\{\frac{L_2\bar{\phi}_0}{A_{11}^0 h}, \frac{L_3\bar{\psi}_0}{A_{11}^0 h}\right\},$$

$$\{\bar{Q}_1, \bar{X}_1, \bar{P}_1\} = \left\{\frac{Q_1\bar{\phi}_0^2}{A_{11}^0 h^2}, \frac{X_1\bar{\phi}_0^2}{A_{11}^0 h^2}, \frac{P_1\bar{\phi}_0^2}{A_{11}^0}\right\},$$

$$\{\bar{Q}_2, \bar{X}_2, \bar{P}_2\} = \left\{\frac{Q_2\bar{\phi}_0\bar{\psi}_0}{A_{11}^0 h^2}, \frac{X_2\bar{\phi}_0\bar{\psi}_0}{A_{11}^0 h^2}, \frac{P_2\bar{\phi}_0\bar{\psi}_0}{A_{11}^0}\right\},$$

$$\{\bar{Q}_3, \bar{X}_3, \bar{P}_3\} = \left\{\frac{Q_3\bar{\psi}_0^2}{A_{11}^0 h^2}, \frac{X_3\bar{\psi}_0^2}{A_{11}^0 h^2}, \frac{P_3\bar{\psi}_0^2}{A_{11}^0}\right\}$$

$$\tag{37}$$

3 Analytical solution for vibration behavior of FG-MEE nanoplates

In the following section, the simply supported boundary conditions are considered on each the four ends of rectangular nanoplate. Thus, the deflections and moments at each end of FG-MEE nanoplate are assumed to be zero. Also, the short circuit type of edge supports which is used for the actuator case is selected for the electric and magnetic potentials (Ansari and Gholami 2016). On the basis of the short circuit type, the electric potential and magnetic potential are supposed to be zero at the ends of FG-MEE nanoplate. Overall, the related boundary conditions can be expressed as

$$\bar{u}(X, 0, \tau) = \bar{u}(X, 1, \tau) = \bar{v}(0, Y, \tau) = \bar{v}(1, Y, \tau) = 0$$

$$\tag{38-1}$$

$$\bar{w}(X, 0, \tau) = \bar{w}(X, 1, \tau) = \bar{w}(0, Y, \tau) = \bar{w}(1, Y, \tau) = 0$$

$$\tag{38-2}$$

$$\bar{\theta}_x(X, 0, \tau) = \bar{\theta}_x(X, 1, \tau) = \bar{\theta}_y(0, Y, \tau) = \bar{\theta}_y(1, Y, \tau) = 0$$

$$\tag{38-3}$$

$$\bar{\phi}(X, 0, \tau) = \bar{\phi}(X, 1, \tau) = \bar{\psi}(0, Y, \tau) = \bar{\psi}(1, Y, \tau) = 0$$

$$\tag{38-4}$$

$$\bar{\phi}(0, Y, \tau) = \bar{\phi}(1, Y, \tau) = \bar{\psi}(X, 0, \tau) = \bar{\psi}(X, 1, \tau) = 0 \tag{38 - 5}$$

$$M_{xx}(0, Y, \tau) = M_{xx}(1, Y, \tau) = M_{yy}(X, 0, \tau) = M_{yy}(X, 1, \tau)$$
$$= 0. \tag{38 - 6}$$

However, the other boundary conditions of engineering interest such as clamped and free boundary conditions can be expressed as

Clamped:

$$\bar{u} = \bar{v} = \bar{\theta}_x = \bar{\theta}_y = \bar{\phi} = \bar{\psi} = 0 \quad \text{at} \quad X = 0, 1; Y = 0, 1 \tag{39}$$

Free:

$$M_{xx} = M_{xy} = Q_{xx} = \bar{\phi} = \bar{\psi} = 0 \quad \text{at } X = 0, 1 \tag{40 - 1}$$

$$M_{yy} = M_{xy} = Q_{yy} = \bar{\phi} = \bar{\psi} = 0 \quad \text{at } Y = 0, 1. \tag{40 - 2}$$

To find more detail about analytically solving governing equations for clamped and free boundary conditions, the reader is referred to (Sobhy 2013; Ebrahimi et al. 2017).

According to Eqs. (38-1–38-6), an analytical approach, so-called Navier solution, is considered to solve dimensionless governing Eqs. (30–36) and obtain the natural frequency and shift frequency. Based on Navier solution and with regards to relation (38-1–38-6), the solutions are presented in the double Fourier series as follows

$$\bar{u}(X, Y, \tau) = e^{i\Omega\tau} \sum_{m=1}^{\infty} \sum_{n=1}^{\infty} \overline{\overline{U}} \cos(m\pi X) \sin(n\pi Y) \tag{41 - 1}$$

$$\bar{v}(X, Y, \tau) = e^{i\Omega\tau} \sum_{m=1}^{\infty} \sum_{n=1}^{\infty} \overline{\overline{V}} \sin(m\pi X) \cos(n\pi Y) \tag{41 - 2}$$

$$\bar{w}(X, Y, \tau) = e^{i\Omega\tau} \sum_{m=1}^{\infty} \sum_{n=1}^{\infty} \overline{\overline{W}} \sin(m\pi X) \sin(n\pi Y) \tag{41 - 3}$$

$$\bar{\theta}_x(X, Y, \tau) = e^{i\Omega\tau} \sum_{m=1}^{\infty} \sum_{n=1}^{\infty} \overline{\overline{\theta}}_x \cos(m\pi X) \sin(n\pi Y) \tag{41 - 4}$$

$$\bar{\theta}_y(X, Y, \tau) = e^{i\Omega\tau} \sum_{m=1}^{\infty} \sum_{n=1}^{\infty} \overline{\overline{\theta}}_y \sin(m\pi X) \cos(n\pi Y) \tag{41 - 5}$$

$$\bar{\phi}(X, Y, \tau) = e^{i\Omega\tau} \sum_{m=1}^{\infty} \sum_{n=1}^{\infty} \overline{\overline{\phi}} \sin(m\pi X) \sin(n\pi Y) \tag{41 - 6}$$

$$\bar{\psi}(X, Y, \tau) = e^{i\Omega\tau} \sum_{m=1}^{\infty} \sum_{n=1}^{\infty} \overline{\overline{\psi}} \sin(m\pi X) \sin(n\pi Y) \tag{41 - 7}$$

in which $i = \sqrt{-1}$ and $\overline{\overline{U}}, \overline{\overline{V}}, \overline{\overline{W}}, \overline{\overline{\theta}}_x, \overline{\overline{\theta}}_y, \overline{\overline{\phi}}, \overline{\overline{\psi}}$ are the unknown coefficients. Also, the half wave numbers through X and Y directions are denoted by symbols m and n, respectively. Furthermore, term Ω refers to the non-dimensional natural frequency of FG-MEE nanoplate. After

applying assumed solutions into Eqs. (30–36), and next multiplying both sides of the resulted error equations by $\sin\left(\frac{m\pi}{l_x}X\right) \sin\left(\frac{n\pi}{l_y}Y\right)$ and integrating over the FG-MEE nanoplate area, yields the following constitutive matrix equation

$$\{[M]\Omega^2 - [K]\}[\Lambda] = 0 \tag{42}$$

in which $[M]$ and $[K]$ demonstrate the mass and stiffness matrices, respectively, and $[\Lambda]$ shows the field variables vector, which are as

$$[M] = \begin{bmatrix} M_{11} & 0 & 0 & M_{14} & 0 & 0 & 0 \\ 0 & M_{22} & 0 & 0 & M_{25} & 0 & 0 \\ 0 & 0 & M_{33} & 0 & 0 & 0 & 0 \\ M_{41} & 0 & 0 & M_{44} & 0 & 0 & 0 \\ 0 & M_{52} & 0 & 0 & M_{55} & 0 & 0 \\ 0 & 0 & 0 & 0 & 0 & 0 & 0 \\ 0 & 0 & 0 & 0 & 0 & 0 & 0 \end{bmatrix},$$

$$[K] = \begin{bmatrix} K_{11} & K_{12} & 0 & K_{14} & K_{15} & K_{16} & K_{17} \\ K_{21} & K_{22} & 0 & K_{24} & K_{25} & K_{26} & K_{27} \\ 0 & 0 & K_{33} & K_{34} & K_{35} & K_{36} & K_{37} \\ K_{41} & K_{42} & K_{43} & K_{44} & K_{45} & K_{46} & K_{47} \\ K_{51} & K_{52} & K_{53} & K_{54} & K_{55} & K_{56} & K_{57} \\ K_{61} & K_{62} & K_{63} & K_{64} & K_{65} & K_{66} & K_{67} \\ K_{71} & K_{72} & K_{73} & K_{74} & K_{75} & K_{76} & K_{77} \end{bmatrix}, \tag{43}$$

$$[\Lambda] = \begin{bmatrix} \overline{\overline{U}} \\ \overline{\overline{V}} \\ \overline{\overline{W}} \\ \overline{\overline{\theta}}_x \\ \overline{\overline{\theta}}_y \\ \overline{\overline{\phi}} \\ \overline{\overline{\psi}} \end{bmatrix}$$

where the elements coefficients of the matrices $[M]$ and $[K]$ are expressed in Appendix B. After calculating the non-trivial solution of equation (42), the natural frequencies can be obtained. For a non-trivial solution, the determinant of the coefficient matrix $\{[M]\Omega^2 - [K]\}$ must be equal to zero, which yields the eigenfrequencies of the system. Moreover, without loss of generality, the resonance frequency with and without considering the effect of attached nanomasses can be respectively presented as $f_{mn} = \frac{\Omega_{mn}}{2\pi}$ and $f_{0,mn} = \frac{\Omega_{0,mn}}{2\pi}$. Now, the natural frequency shift can be defined as follows

$$\Delta f_{mn} = f_{0,mn} - f_{mn}. \tag{44}$$

4 Numerical examples and discussions

4.1 Convergence and comparison study

Before embarking on the investigation of the variations of the suggested system frequency shift, some convergence analyses to determine the accuracy of the developed model are performed. Firstly, after eliminating Pasternak substrate and FGMs, the calculated the first two non-dimensional natural frequencies of MEE nanoplate for different nonlocal parameters based on current study are illustrated in Table 1 along with predictions according to the nonlocal Mindlin plate theory (MPT) (Ansari and Gholami 2016) and nonlocal Kirchhoff plate theory (KPT) (Ke et al. 2014). It is clear from Table 1 that proposed model results are in great agreement with those reported by (Ke et al. 2014; Ansari and Gholami 2016).

Another comparison study is also carried out through Fig. 2 in which the fundamental frequency shift calculated according to the present model for different values of nonlocal parameter and different added particles at location $x_1 = 0.5l_x, y_1 = 0.5l_y$ without considering FGMs, Pasternak medium, and piezomagnetic effect, are compared to those of piezoelectric Kirchhoff nanoplate model of Asemi et al. (2015). Figure 2 denotes an excellent agreement between the outcomes of current paper and the results of Ref. (Asemi et al. 2015).

4.2 Benchmark results

In this subsection, the benchmark results are presented in the tabular and graphical form to better understanding and explaining the significant parameters such as the position of single or multiple attached masses on the natural frequency shift changes. To achieve this goal, we consider the three different configurations (single mass, two masses, and four masses) for the number of added particles. It is assumed that the total mass of added masses is identical for each state. However, the details of these three cases are given in Table 2. Furthermore, it is supposed that FG-MEE nanoplate to be composed of barium titanate (BaTiO$_3$) and cobalt iron oxide (CoFe$_2$O$_4$) with effective material characteristics given in Table 3 (Aboudi 2001). Moreover, the utilized geometrical characteristics of nanoplate are assumed to be as $h = 1$ nm, $l_x = l_y = 10$ nm, and half wave numbers are assumed to be $m = n = 1$.

Initially, to study the influences of length to thickness ratio and material property gradient index on the changes of frequency shift, Table 4 is provided for the three figurations of the attached nanoparticles. Here, we took $\bar{K}_w = \bar{K}_G = \phi_0 = \psi_0 = 0, \mu = 0.2, m_{Total} = 10^{-21}$ kg, R = 1. It is clear that an increase in the volume fraction of barium titanate part (BaTiO$_3$)/cobalt iron oxide component (CoFe$_2$O$_4$) leads to decreasing/increasing the bending stiffness of FG-MEE nanoplate, and consequently, frequency shift or sensibility efficiency of nanosensor decrease/increases. Furthermore, another remarkable point derived from this table is that the sensitivity property of the nanosensor reduces by increasing the number of added masses. Also, it can be found that frequency shift significantly decreases as the length to thickness ratio increases.

Figure 3 gives a comparison of variations of frequency shift against to the total attached mass for different values of the nonlocal parameter, $\bar{K}_w = \bar{K}_G = \phi_0 = \psi_0 = 0, R = K = 1$. The most important distinctions are as follows. It is observed that by taking into account the large values of the nonlocal parameter, the sensitivity performance of nanosensor reduces, particularly for large values of total attached mass (mainly due to the softening effect of the nonlocal parameter on the nanostructures). Furthermore, it is demonstrated that increasing the total attached mass value from 10^{-21} to 10^{-19}kg leads to a notable increase in the frequency shift of FG-MEE nanoplate. Moreover, it can be resulted from this figure that the influence of various figurations of attached nanoparticles on the frequency shift become lower for large values of the total attached mass and the nonlocal parameter. It is also found that for large values of nonlocal parameter, FG-MEE nanosensor is insensitive to the variation of the total attached mass.

Depicted in Fig. 4 is the influence of the aspect ratio on the sensing property of FG-MEE nanosensor for different values of the total attached mass, $\bar{K}_w = \bar{K}_G = \phi_0 = \psi_0 = 0, \mu = 0.2, K = 1$. As can be seen, an increase in the aspect ratio causes to monotonically decreasing the frequency shift of FG-MEE nanoplate and the ability of nanosensor to sense attached particles reduces. Also, it is clear that the case of single mass has the maximum value of frequency shift.

To study the effects of the transverse and shear stiffness parameters of Pasternak elastic substrate on the sensitivity performance of FG-MEE nanosensor, Figure 5 is plotted. Here, we did not consider the external electric and external magnetic potentials, and the nonlocal parameter is supposed to be 0.2. In particular, it is easily deduced that by taking into account stiffer polymer matrix, sensitivity property of nanosensor increases. Furthermore, it is noticed that under the maximum value of the total attached mass, the influence of Pasternak foundation on the frequency shift increases.

Figure 6 reveals the influence of the applied external electric voltage on the frequency shift curves versus the total attached mass for the three cases of mass, $\bar{K}_w = \bar{K}_G = \psi_0 = 0, \mu = 0.2, K = R = 1$. The most

interesting result is perhaps the fact that a rise in the value of the electric voltage form −0.2 to 0.05 V causes a decrease in the sensitivity behavior of FG-MEE nanosensor. This may be explained by the fact that imposing the positive (negative) applied external electric potential, the compressive (tensile) in-plane loads tend to generate in FG-MEE nanosensor, and consequently, frequency shift reduces (increases). Furthermore, it is found from figure that when FG-MEE nanosensor is subjected to the positive external electric potential, the influence of the total attached mass on the sensitivity property remarkably become low.

The frequency shift curves of FG-MEE nanosensor with respect to the total attached mass for different values of external magnetic potential are displayed in Fig. 7. Here, we took $\bar{K}_w = \bar{K}_G = \psi_0 = 0, \mu = 0.2, K = R = 1$. It is illustrated that contrary to the influence of external electric voltage on the variation of frequency shift, by increasing external magnetic potential from −0.01 to 0.02 A, the sensitivity property of FG-MEE nanoplate according to the mass sensor considerably increases. Also, it should be noted that when FG-MEE nanosensor is subjected to the negative external magnetic potential, the effect of the total attached mass on the sensitivity property significantly become low.

Figure 8a–d show the effect of the higher modes on the difference between the natural frequency of FG-MEE nanoplate with and without added nanoparticle corresponding to the different positions of single attached nanoparticle. The results are calculated for $\bar{K}_w = \bar{K}_G = \psi_0 = \phi_0 = 0, \mu = 0.2, K = R = 1, m_{Total} = 10^{-20}$kg. It can be seen that the sensitivity property of nanosensor increases when the attached nanoparticle is closer to the center of FG-MEE nanoplate. This implies that the sensitivity property of nanosensor vanishes when added nanoparticle is located at the edges of FG-MEE nanoplate. Moreover, it is denoted that by increasing mode number the frequency shift remarkably increases.

5 Concluding remarks

The main contribution of the current study was to provide a nanosize mass detection model basis on the vibrating FG-MEE Mindlin nanoplate resting on Pasternak foundation. Also, external electric voltage and external magnetic potential were exerted to the FG-MEE nanosensor. Eringen's differential constitutive law was employed to take into account small-scale effect into the constitutive equations. By using the power law distribution, the effective material properties of rectangular FG-MEE nanoplate change gradually in the direction of nanoplate thickness. Hamilton's principle was utilized in conjunction with nonlocal Mindlin plate theory to derive the size-dependent governing partial differential equations of motion. Afterward, outlined discussions were depicted to demonstrate how to change the sensitivity property of FG-MEE nanosensor by varying the position of attached nanoparticle, the number of nanoparticles, the values of the nonlocal parameter, initial external electric and magnetic potentials, material property gradient index, the dimension of the FG-MEE nanoplate, and Pasternak substrate coefficients. Some noteworthy points derived from numerical results can be listed as

- The difference between the natural frequency of FG-MEE nanoplate with and without attached nanoparticle notable increases by increasing external magnetic potential.
- The sensitivity performance of FG-MEE nanosensor reduces under an increase of external electric voltage.
- An increase in the value of the volume fraction exponent causes higher frequency shift.
- It is demonstrated that nonlocal component has a considerable reduction on the sensibility of FG-MEE nanosensor.

Appendix A

$$\{A_{11}, B_{11}, D_{11}\} = \int_{-\frac{h}{2}}^{\frac{h}{2}} \bar{C}_{11}(z)\{1, z, z^2\}dz, \{A_{12}, B_{12}, D_{12}\}$$

$$= \int_{-\frac{h}{2}}^{\frac{h}{2}} \bar{C}_{12}(z)\{1, z, z^2\}dz,$$

$$\{A_{22}, B_{22}, D_{22}\} = \int_{-\frac{h}{2}}^{\frac{h}{2}} \bar{C}_{22}(z)\{1, z, z^2\}dz, \{A_{66}, B_{66}, D_{66}\}$$

$$= \int_{-\frac{h}{2}}^{\frac{h}{2}} \bar{C}_{66}(z)\{1, z, z^2\}dz,$$

$$A_{55} = \int_{-\frac{h}{2}}^{\frac{h}{2}} \bar{C}_{55}(z)dz, A_{44} = \int_{-\frac{h}{2}}^{\frac{h}{2}} \bar{C}_{44}(z)dz, \{E_{11}, E_{22}\}$$

$$= \int_{-\frac{h}{2}}^{\frac{h}{2}} \bar{e}_{31}(z)\left(\frac{\pi}{h}\right)sin\left(\frac{\pi}{h}z\right)\{1, z\}dz,$$

$$\{F_{11}, F_{22}\} = \int_{-\frac{h}{2}}^{\frac{h}{2}} \bar{q}_{31}(z)\left(\frac{\pi}{h}\right)sin\left(\frac{\pi}{h}z\right)\{1,z\}dz, \{G_{11}, G_{22}\}$$

$$= \int_{-\frac{h}{2}}^{\frac{h}{2}} e_{32}(z)\left(\frac{\pi}{h}\right)sin\left(\frac{\pi}{h}z\right)\{1,z\}dz, \{H_{11}, H_{22}\}$$

$$= \int_{-\frac{h}{2}}^{\frac{h}{2}} \bar{q}_{32}(z)\left(\frac{\pi}{h}\right)sin\left(\frac{\pi}{h}z\right)\{1,z\}dz,$$

$$J_2 = \int_{-\frac{h}{2}}^{\frac{h}{2}} e_{15}(z)cos\left(\frac{\pi}{h}z\right)dz, \quad J_3 = \int_{-\frac{h}{2}}^{\frac{h}{2}} \bar{q}_{15}(z)$$
$$cos\left(\frac{\pi}{h}z\right)dz,$$

$$L_2 = \int_{-\frac{h}{2}}^{\frac{h}{2}} e_{24}(z)cos\left(\frac{\pi}{h}z\right)dz, \quad L_3 = \int_{-\frac{h}{2}}^{\frac{h}{2}} \bar{q}_{24}(z)$$
$$cos\left(\frac{\pi}{h}z\right)dz,$$

$$Q_1 = \int_{-\frac{h}{2}}^{\frac{h}{2}} \bar{\eta}_{11}(z)\left[cos\left(\frac{\pi}{h}z\right)\right]^2 dz, \quad Q_2 = \int_{-\frac{h}{2}}^{\frac{h}{2}} \bar{d}_{11}(z)$$
$$\left[cos\left(\frac{\pi}{h}z\right)\right]^2 dz,$$

$$X_1 = \int_{-\frac{h}{2}}^{\frac{h}{2}} \bar{\eta}_{22}(z)\left[cos\left(\frac{\pi}{h}z\right)\right]^2 dz, \quad X_2 = \int_{-\frac{h}{2}}^{\frac{h}{2}} \bar{d}_{22}(z)$$
$$\left[cos\left(\frac{\pi}{h}z\right)\right]^2 dz,$$

$$P_1 = \int_{-\frac{h}{2}}^{\frac{h}{2}} \bar{\eta}_{33}(z)\left[\left(\frac{\pi}{h}\right)sin\left(\frac{\pi}{h}z\right)\right]^2 dz, \quad P_2 = \int_{-\frac{h}{2}}^{\frac{h}{2}} \bar{d}_{33}(z)$$
$$\left[\left(\frac{\pi}{h}\right)sin\left(\frac{\pi}{h}z\right)\right]^2 dz$$

$$Q_3 = \int_{-\frac{h}{2}}^{\frac{h}{2}} \bar{\mu}_{11}(z)\left[cos\left(\frac{\pi}{h}z\right)\right]^2 dz, \quad X_3 = \int_{-\frac{h}{2}}^{\frac{h}{2}} \bar{\mu}_{22}(z)$$
$$\left[cos\left(\frac{\pi}{h}z\right)\right]^2 dz,$$

$$P_3 = \int_{-\frac{h}{2}}^{\frac{h}{2}} \bar{\mu}_{33}(z)\left[\left(\frac{\pi}{h}\right)sin\left(\frac{\pi}{h}z\right)\right]^2 dz,$$

$$\{N_{xx1}^E, N_{xx2}^E\} = \int_{-\frac{h}{2}}^{\frac{h}{2}} 2\bar{e}_{31}(z)\frac{\phi_0}{h}\{1,z\}dz,$$

$$\{N_{xx1}^M, N_{xx2}^M\} = \int_{-\frac{h}{2}}^{\frac{h}{2}} 2\bar{q}_{31}(z)\frac{\psi_0}{h}\{1,z\}dz,$$

$$\{N_{yy1}^E, N_{yy2}^E\} = \int_{-\frac{h}{2}}^{\frac{h}{2}} 2\bar{e}_{32}(z)\frac{\phi_0}{h}\{1,z\}dz,$$

$$\{N_{yy1}^M, N_{yy2}^M\} = \int_{-\frac{h}{2}}^{\frac{h}{2}} 2\bar{q}_{32}(z)\frac{\psi_0}{h}\{1,z\}dz,$$

$$N_{xx3}^E = \int_{-\frac{h}{2}}^{\frac{h}{2}} 2\bar{\eta}_{33}(z)\frac{\phi_0\pi}{h^2}sin\left(\frac{\pi}{h}z\right)dz,$$

$$N_{xx3}^M = \int_{-\frac{h}{2}}^{\frac{h}{2}} 2\bar{d}_{33}(z)\frac{\psi_0\pi}{h^2}sin\left(\frac{\pi}{h}z\right)dz,$$

$$N_{yy3}^E = \int_{-\frac{h}{2}}^{\frac{h}{2}} 2\bar{d}_{33}(z)\frac{\phi_0\pi}{h^2}sin\left(\frac{\pi}{h}z\right)dz,$$

$$N_{yy3}^M = \int_{-\frac{h}{2}}^{\frac{h}{2}} 2\bar{\mu}_{33}(z)\frac{\psi_0\pi}{h^2}sin\left(\frac{\pi}{h}z\right)dz.$$

Appendix B

The elements coefficient of the matrices M_{ij}, K_{ij} are

$$M_{11} = M_{22} = \left[1+\mu^2\left((m\pi)^2+R^2(n\pi)^2\right)\right]\frac{I_0}{I_0^0},$$

$$M_{14} = M_{41} = M_{25} = M_{52} = \left[1+\mu^2\left((m\pi)^2+R^2(n\pi)^2\right)\right]\frac{I_1}{I_0^0 h},$$

$$M_{33} = \frac{1}{r}\left[1+\mu^2\left((m\pi)^2+R^2(n\pi)^2\right)\right]$$
$$\left[\frac{I_0}{I_0^0}+4\sum_{e=1}^{p}\frac{m_e}{I_0^0 l_x l_y}sin^2(m\pi X_e)sin^2(n\pi Y_l)\right],$$

$$M_{44} = M_{55} = \left[1+\mu^2\left((m\pi)^2+R^2(n\pi)^2\right)\right]\frac{I_2}{I_0^0 h^2},$$

$$K_{11} = \bar{A}_{11}(m\pi)^2 + \bar{A}_{66}R^2(n\pi)^2, \quad K_{12} = K_{21} = (\bar{A}_{12} + \bar{A}_{66})R(m\pi)(n\pi),$$

$$K_{14} = K_{41} = \bar{B}_{11}(m\pi)^2 + \bar{B}_{66}R^2(n\pi)^2,$$

$$K_{15} = K_{24} = K_{42} = K_{51} = (\bar{B}_{12} + \bar{B}_{66})R(m\pi)(n\pi),$$

$$K_{16} = -\bar{E}_{11}r(m\pi), \quad K_{17} = -\bar{F}_{11}r(m\pi), \quad K_{22} = \bar{A}_{66}(m\pi)^2 + \bar{A}_{22}R^2(n\pi)^2,$$

$$K_{25} = K_{52} = \bar{B}_{66}(m\pi)^2 + \bar{B}_{22}R^2(n\pi)^2, \quad K_{26} = -\bar{G}_{11}Rr(n\pi),$$

$$K_{27} = -\bar{H}_{11}Rr(n\pi), \quad K_{33} = \frac{k_s\bar{A}_{55}}{r}(m\pi)^2 + \frac{k_s\bar{A}_{44}R^2}{r}(n\pi)^2$$
$$+ \frac{1}{r}\left[1 + \mu^2\left((m\pi)^2 + R^2(n\pi)^2\right)\right]$$
$$\left[\frac{(N_{Ex} + N_{Mx})}{A^0_{11}}(m\pi)^2 + \frac{(N_{Ey} + N_{My})R^2}{A^0_{11}}(n\pi)^2 + \bar{K}_w\right.$$
$$\left.+ \bar{K}_G\left((m\pi)^2 + R^2(n\pi)^2\right)\right], \quad K_{34} = k_s\bar{A}_{55}(m\pi), \quad K_{35} = k_s\bar{A}_{44}R(n\pi),$$

$$K_{36} = -k_s\frac{\bar{J}_2}{r}(m\pi)^2 - k_s\frac{\bar{L}_2R^2}{r}(n\pi)^2,$$

$$K_{37} = -k_s\frac{\bar{J}_3}{r}(m\pi)^2 - k_s\frac{\bar{L}_3R^2}{r}(n\pi)^2, \quad K_{43} = k_s\bar{A}_{55}r(m\pi),$$

$$K_{44} = \bar{D}_{11}(m\pi)^2 + \bar{D}_{66}R^2(n\pi)^2 + k_s\bar{A}_{55}r^2,$$

$$K_{45} = K_{54} = (\bar{D}_{12} + \bar{D}_{66})R(m\pi)(n\pi),$$

$$K_{46} = -(\bar{E}_{22} + k_s\bar{J}_2)r(m\pi),$$

$$K_{47} = -(\bar{F}_{22} + k_s\bar{J}_3)r(m\pi), \quad K_{53} = k_s\bar{A}_{44}rR(n\pi),$$

$$K_{55} = \bar{D}_{66}(m\pi)^2 + \bar{D}_{22}R^2(n\pi)^2 + k_s\bar{A}_{44}r^2,$$

$$K_{56} = -(\bar{G}_{22} + k_s\bar{L}_2)Rr(n\pi), \quad K_{57} = -(\bar{H}_{22} + k_s\bar{L}_3)Rr(n\pi),$$

$$K_{61} = -\bar{E}_{11}(m\pi), \quad K_{62} = -\bar{G}_{11}R(n\pi),$$

$$K_{63} = -\frac{\bar{J}_2}{r}(m\pi)^2 - \frac{\bar{L}_2R^2}{r}(n\pi)^2,$$

$$K_{64} = -(\bar{E}_{22} + \bar{J}_2)(m\pi), \quad K_{65} = -(\bar{G}_{22} + \bar{L}_2)R(n\pi),$$

$$K_{66} = -\frac{1}{r}\bar{Q}_1(m\pi)^2 - \frac{R^2}{r}\bar{X}_1(n\pi)^2 - \bar{P}_1r,$$

$$K_{67} = K_{76} = -\frac{1}{r}\bar{Q}_2(m\pi)^2 - \frac{R^2}{r}\bar{X}_2(n\pi)^2 - \bar{P}_2r,$$

$$K_{71} = -\bar{F}_{11}(m\pi), \quad K_{72} = -\bar{H}_{11}R(n\pi),$$

$$K_{73} = -\frac{\bar{J}_3}{r}(m\pi)^2 - \frac{\bar{L}_3R^2}{r}(n\pi)^2,$$

$$K_{74} = -(\bar{F}_{22} + \bar{J}_3)(m\pi), \quad K_{75} = -(\bar{H}_{22} + k_s\bar{L}_3)R(n\pi),$$

$$K_{76} = -\frac{1}{r}\bar{Q}_3(m\pi)^2 - \frac{R^2}{r}\bar{X}_3(n\pi)^2 - \bar{P}_3r.$$

References

Aboudi J (2001) Micromechanical analysis of fully coupled electro-magneto-thermo-elastic multiphase composites. Smart Mater Struct 10:867–877. https://doi.org/10.1088/0964-1726/10/5/303

Akdogan EK, Allahverdi M, Safari A (2005) Piezoelectric composites for sensor and actuator applications. IEEE Trans Ultrason Ferroelectr Freq Control 52:746–775. https://doi.org/10.1109/TUFFC.2005.1503962

Alluri NR, Saravanakumar B, Kim S-J (2015) Flexible, hybrid piezoelectric film (BaTi$_{(1-x)}$ Zr$_x$O$_3$)/PVDF nanogenerator as a self-powered fluid velocity sensor. ACS Appl Mater Interfaces 7:9831–9840. https://doi.org/10.1021/acsami.5b01760

Ansari R, Gholami R (2016) Nonlocal free vibration in the pre- and post-buckled states of magneto-electro-thermo elastic rectangular nanoplates with various edge conditions. Smart Mater Struct 25:95033. https://doi.org/10.1088/0964-1726/25/9/095033

Ansari R, Gholami R (2017) Size-dependent buckling and postbuckling analyses of first-order shear deformable magneto-electro-thermo elastic nanoplates based on the nonlocal elasticity theory. Int J Struct Stab Dyn 17:1750014. https://doi.org/10.1142/s0219455417500146

Ansari R, Sahmani S, Arash B (2010) Nonlocal plate model for free vibrations of single-layered graphene sheets. Phys Lett A 375:53–62. https://doi.org/10.1016/j.physleta.2010.10.028

Ansari R, Faghih Shojaei M, Ebrahimi F, Rouhi H (2015a) A non-classical Timoshenko beam element for the postbuckling analysis of microbeams based on Mindlin's strain gradient theory. Arch Appl Mech 85:937–953. https://doi.org/10.1007/s00419-015-1002-y

Ansari R, Gholami R, Rouhi H (2015b) Size-dependent nonlinear forced vibration analysis of magneto-electro-thermo-elastic Timoshenko nanobeams based upon the nonlocal elasticity theory. Compos Struct 126:216–226. https://doi.org/10.1016/j.compstruct.2015.02.068

Ansari R, Hasrati E, Gholami R, Sadeghi F (2015c) Nonlinear analysis of forced vibration of nonlocal third-order shear deformable beam model of magneto–electro–thermo elastic nanobeams. Compos Part B Eng 83:226–241. https://doi.org/10.1016/j.compositesb.2015.08.038

Apuzzo A, Barretta R, Luciano R et al (2017) Free vibrations of Bernoulli–Euler nano-beams by the stress-driven nonlocal integral model. Compos Part B Eng 123:105–111. https://doi.org/10.1016/J.COMPOSITESB.2017.03.057

Asemi HR, Asemi SR, Farajpour A, Mohammadi M (2015) Nanoscale mass detection based on vibrating piezoelectric ultrathin films under thermo-electro-mechanical loads. Phys E Low Dimens Syst Nanostruct 68:112–122. https://doi.org/10.1016/j.physe.2014.12.025

Baker A, Dutton S, Kelly D (2004) Composite materials for aircraft structures, 2nd edn. AIAA Inc, Virginia

Barati MR, Shahverdi H, Zenkour AM (2017) Electro-mechanical vibration of smart piezoelectric FG plates with porosities according to a refined four-variable theory. Mech Adv Mater Struct 24:987–998

Barretta R, Feo L, Luciano R et al (2016) Functionally graded Timoshenko nanobeams: a novel nonlocal gradient formulation. Compos Part B Eng 100:208–219. https://doi.org/10.1016/j.compositesb.2016.05.052

Chen CQ, Shi Y, Zhang YS et al (2006) Size dependence of Young's modulus in ZnO nanowires. Phys Rev Lett 96:75505. https://doi.org/10.1103/PhysRevLett.96.075505

Ebrahimi F, Jafari A, Barati MR (2017) Vibration analysis of magneto-electro-elastic heterogeneous porous material plates resting on elastic foundations. Thin Walled Struct 119:33–46. https://doi.org/10.1016/J.TWS.2017.04.002

Eringen AC (1972) Linear theory of nonlocal elasticity and dispersion of plane waves. Int J Eng Sci 10:425–435. https://doi.org/10.1016/0020-7225(72)90050-X

Eringen AC (1983) On differential equations of nonlocal elasticity and solutions of screw dislocation and surface waves. J Appl Phys 54:4703. https://doi.org/10.1063/1.332803

Farajpour A, Hairi Yazdi MR, Rastgoo A et al (2016) Nonlocal nonlinear plate model for large amplitude vibration of magneto-electro-elastic nanoplates. Compos Struct 140:323–336. https://doi.org/10.1016/j.compstruct.2015.12.039

Guo W, Liu T, Zhang H et al (2012) Gas-sensing performance enhancement in ZnO nanostructures by hierarchical morphology. Sens Actuators B Chem 166:492–499. https://doi.org/10.1016/j.snb.2012.02.093

Hosseini M, Jamalpoor A (2015) Analytical solution for thermomechanical vibration of double-viscoelastic nanoplate-systems made of functionally graded materials. J Therm Stress 38:1428–1456. https://doi.org/10.1080/01495739.2015.1073986

Hosseini M, Jamalpoor A, Fath A (2016a) Surface effect on the biaxial buckling and free vibration of FGM nanoplate embedded in visco-Pasternak standard linear solid-type of foundation. Meccanica. https://doi.org/10.1007/s11012-016-0469-0

Hosseini M, Bahreman M, Jamalpoor A (2016b) Using the modified strain gradient theory to investigate the size-dependent biaxial buckling analysis of an orthotropic multi-microplate system. Acta Mech 227:1621–1643. https://doi.org/10.1007/s00707-016-1570-0

Hosseini M, Jamalpoor A, Bahreman M (2016c) Small-scale effects on the free vibrational behavior of embedded viscoelastic double-nanoplate-systems under thermal environment. Acta Astronaut 129:400–409. https://doi.org/10.1016/j.actaastro.2016.10.001

Hosseini M, Bahreman M, Jamalpoor A (2017) Thermomechanical vibration analysis of FGM viscoelastic multi-nanoplate system incorporating the surface effects via nonlocal elasticity theory. Microsyst Technol 23:3041–3058. https://doi.org/10.1007/s00542-016-3133-7

Jalali SK, Naei MH, Pugno NM (2015) A mixed approach for studying size effects and connecting interactions of planar nano structures as resonant mass sensors. Microsyst Technol 21:2375–2386. https://doi.org/10.1007/s00542-014-2362-x

Jamalpoor A, Kiani A (2017) Vibration analysis of bonded double-FGM viscoelastic nanoplate systems based on a modified strain gradient theory incorporating surface effects. Appl Phys A 123:201. https://doi.org/10.1007/s00339-017-0784-x

Jamalpoor A, Ahmadi-Savadkoohi A, Hosseini M, Hosseini-Hashemi S (2017) Free vibration and biaxial buckling analysis of double magneto-electro-elastic nanoplate-systems coupled by a visco-Pasternak medium via nonlocal elasticity theory. Eur J Mech A/Solids 63:84–98

Karličić D, Kozić P, Adhikari S et al (2015) Nonlocal mass-nanosensor model based on the damped vibration of single-layer graphene sheet influenced by in-plane magnetic field. Int J Mech Sci 96:132–142. https://doi.org/10.1016/j.ijmecsci.2015.03.014

Ke L-L, Wang Y-S (2014) Free vibration of size-dependent magneto-electro-elastic nanobeams based on the nonlocal theory. Phys E Low Dimens Syst Nanostruct 63:52–61. https://doi.org/10.1016/j.physe.2014.05.002

Ke L-L, Wang Y-S, Yang J, Kitipornchai S (2014) Free vibration of size-dependent magneto-electro-elastic nanoplates based on the nonlocal theory. Acta Mech Sin 30:516–525. https://doi.org/10.1007/s10409-014-0072-3

Kiani A, Sheikhkhoshkar M, Jamalpoor A, Khanzadi M (2017) Free vibration problem of embedded magneto-electro-thermo-elastic nanoplate made of functionally graded materials via nonlocal third-order shear deformation theory. J Intell Mater Syst Struct. https://doi.org/10.1177/1045389X17721034

Kim CH, Myung Y, Cho YJ et al (2009) Electronic structure of vertically aligned Mn-doped $CoFe_2O_4$ nanowires and their application as humidity sensors and photodetectors. J Phys Chem C 113:7085–7090. https://doi.org/10.1021/jp900165c

Kumar S, Murthy Reddy KVVS, Kumar A, Rohini Devi G (2013) Development and characterization of polymer–ceramic continuous fiber reinforced functionally graded composites for aerospace application. Aerosp Sci Technol 26:185–191. https://doi.org/10.1016/j.ast.2012.04.002

Lam DCC, Yang F, Chong ACM et al (2003) Experiments and theory in strain gradient elasticity. J Mech Phys Solids 51:1477–1508. https://doi.org/10.1016/S0022-5096(03)00053-X

Li C, Thostenson ET, Chou T-W (2008) Sensors and actuators based on carbon nanotubes and their composites: a review. Compos Sci Technol 68:1227–1249. https://doi.org/10.1016/j.compscitech.2008.01.006

Li YS, Cai ZY, Shi SY (2014) Buckling and free vibration of magnetoelectroelastic nanoplate based on nonlocal theory. Compos Struct 111:522–529. https://doi.org/10.1016/j.compstruct.2014.01.033

Li Y, Ma P, Wang W (2016) Bending, buckling, and free vibration of magnetoelectroelastic nanobeam based on nonlocal theory. J Intell Mater Syst Struct 27:1139–1149. https://doi.org/10.1177/1045389X15585899

Liu J, Zhang P, Lin G et al (2016) High order solutions for the magneto-electro-elastic plate with non-uniform materials. Int J Mech Sci 115:532–551. https://doi.org/10.1016/j.ijmecsci.2016.07.033

Ma L-H, Ke L-L, Wang Y-Z, Wang Y-S (2017) Wave propagation in magneto-electro-elastic nanobeams via two nonlocal beam models. Phys E Low Dimens Syst Nanostruct 86:253–261. https://doi.org/10.1016/j.physe.2016.10.036

Mechab I, Mechab B, Benaissa S, Serier B, Bouiadjra BB (2016) Free vibration analysis of FGM nanoplate with porosities resting on Winkler Pasternak elastic foundations based on two-variable refined plate theories. J Braz Soc Mech Sci Eng 38:2193–2211

Müller E, Drašar Č, Schilz J, Kaysser W (2003) Functionally graded materials for sensor and energy applications. Mater Sci Eng A 362:17–39. https://doi.org/10.1016/S0921-5093(03)00581-1

Narendar S (2016) Wave dispersion in functionally graded magneto-electro-elastic nonlocal rod. Aerosp Sci Technol 51:42–51. https://doi.org/10.1016/j.ast.2016.01.012

Natarajan S, Chakraborty S, Thangavel M et al (2012) Size-dependent free flexural vibration behavior of functionally graded nanoplates. Comput Mater Sci 65:74–80. https://doi.org/10.1016/j.commatsci.2012.06.031

Parthasarathy J, Starly B, Raman S (2011) A design for the additive manufacture of functionally graded porous structures with tailored mechanical properties for biomedical applications. J Manuf Process 13:160–170. https://doi.org/10.1016/j.jmapro.2011.01.004

Pompe W, Worch H, Epple M et al (2003) Functionally graded materials for biomedical applications. Mater Sci Eng A 362:40–60. https://doi.org/10.1016/S0921-5093(03)00580-X

Pradhan SC, Phadikar JK (2009) Nonlocal elasticity theory for vibration of nanoplates. J Sound Vib 325:206–223. https://doi.org/10.1016/j.jsv.2009.03.007

Rahimi GH, Arefi M, Khoshgoftar MJ (2011) Application and analysis of functionally graded piezoelectrical rotating cylinder as mechanical sensor subjected to pressure and thermal loads. Appl Math Mech 32:997–1008. https://doi.org/10.1007/s10483-011-1475-6

Ramirez F, Heyliger PR, Pan E (2006) Discrete layer solution to free vibrations of functionally graded magneto-electro-elastic plates. Mech Adv Mater Struct 13:249–266

Razavi S, Shooshtari A (2015) Nonlinear free vibration of magneto-electro-elastic rectangular plates. Compos Struct 119:377–384. https://doi.org/10.1016/j.compstruct.2014.08.034

Romano G, Barretta R (2016) Comment on the paper "Exact solution of Eringen's nonlocal integral model for bending of Euler–

Bernoulli and Timoshenko beams" by Meral Tuna & Mesut Kirca. Int J Eng Sci 109:240–242. https://doi.org/10.1016/j.ijengsci.2016.09.009

Romano G, Barretta R (2017a) Stress-driven versus strain-driven nonlocal integral model for elastic nano-beams. Compos Part B Eng 114:184–188. https://doi.org/10.1016/J.COMPOSITESB.2017.01.008

Romano G, Barretta R (2017b) Nonlocal elasticity in nanobeams: the stress-driven integral model. Int J Eng Sci 115:14–27. https://doi.org/10.1016/J.IJENGSCI.2017.03.002

Romano G, Barretta R, Diaco M (2017a) On nonlocal integral models for elastic nano-beams. Int J Mech Sci 131–132:490–499. https://doi.org/10.1016/J.IJMECSCI.2017.07.013

Romano G, Barretta R, Diaco M, Marotti de Sciarra F (2017b) Constitutive boundary conditions and paradoxes in nonlocal elastic nanobeams. Int J Mech Sci 121:151–156. https://doi.org/10.1016/J.IJMECSCI.2016.10.036

Sadeghzadeh S (2016) Nanoparticle mass detection by single and multilayer graphene sheets: theory and simulations. Appl Math Model 40:7862–7879. https://doi.org/10.1016/j.apm.2016.03.051

Shen Z-B, Tang H-L, Li D-K, Tang G-J (2012) Vibration of single-layered graphene sheet-based nanomechanical sensor via nonlocal Kirchhoff plate theory. Comput Mater Sci 61:200–205. https://doi.org/10.1016/j.commatsci.2012.04.003

Shi J-X, Liu Y, Shimoda M (2015) Vibration analysis of a carbyne-based resonator in nano-mechanical mass sensors. J Phys D Appl Phys 48:115303. https://doi.org/10.1088/0022-3727/48/11/115303

Shirbani MM, Shishesaz M, Sedighi HM, Hajnayeb A (2017) Parametric modeling of a novel longitudinal vibration-based energy harvester using magneto-electro-elastic materials. Microsyst Technol 23:5989–6004. https://doi.org/10.1007/s00542-017-3402-0

Shooshtari A, Razavi S (2016) Vibration of a multiphase magneto-electro-elastic simply supported rectangular plate subjected to harmonic forces. J Intell Mater Syst Struct. https://doi.org/10.1177/1045389X16649451

Sobhy M (2013) Buckling and free vibration of exponentially graded sandwich plates resting on elastic foundations under various boundary conditions. Compos Struct 99:76–87. https://doi.org/10.1016/J.COMPSTRUCT.2012.11.018

Stan G, Ciobanu CV, Parthangal PM, Cook RF (2007) Diameter-dependent radial and tangential elastic moduli of ZnO nanowires. Nano Lett 7:3691–3697. https://doi.org/10.1021/nl071986e

Taei M, Hasanpour F, Salavati H, Mohammadian S (2016) Fast and sensitive determination of doxorubicin using multi-walled carbon nanotubes as a sensor and $CoFe_2O_4$ magnetic nanoparticles as a mediator. Microchim Acta 183:49–56. https://doi.org/10.1007/s00604-015-1588-3

Thang PT, Nguyen T-T, Lee J (2017) A new approach for nonlinear buckling analysis of imperfect functionally graded carbon nanotube-reinforced composite plates. Compos Part B Eng 127:166–174. https://doi.org/10.1016/j.compositesb.2016.12.002

Tressler JF, Alkoy S, Dogan A, Newnham RE (1999) Functional composites for sensors, actuators and transducers. Compos Part A Appl Sci Manuf 30:477–482. https://doi.org/10.1016/S1359-835X(98)00137-7

Vaezi M, Shirbani MM, Hajnayeb A (2016) Free vibration analysis of magneto-electro-elastic microbeams subjected to magneto-electric loads. Phys E Low Dimens Syst Nanostructures 75:280–286. https://doi.org/10.1016/j.physe.2015.09.019

Van Den Boomgaard J, Terrell DR, Born RAJ, Giller HFJI (1974) An in situ grown eutectic magnetoelectric composite material. J Mater Sci 9:1705–1709. https://doi.org/10.1007/BF00540770

Wang W, Li P, Jin F (2016) Two-dimensional linear elasticity theory of magneto-electro-elastic plates considering surface and nonlocal effects for nanoscale device applications. Smart Mater Struct 25:95026. https://doi.org/10.1088/0964-1726/25/9/095026

Wu CP, Tsai YH (2007) Static behavior of functionally graded magneto-electro-elastic shells under electric displacement and magnetic flux. Int J Eng Sci 45:744–769. https://doi.org/10.1016/j.ijengsci.2007.05.002

Wu C-P, Chen S-J, Chiu K-H (2010) Three-dimensional static behavior of functionally graded magneto-electro-elastic plates using the modified Pagano method. Mech Res Commun 37:54–60. https://doi.org/10.1016/j.mechrescom.2009.10.003

Wu B, Zhang C, Chen W, Zhang C (2015) Surface effects on anti-plane shear waves propagating in magneto-electro-elastic nanoplates. Smart Mater Struct 24:95017. https://doi.org/10.1088/0964-1726/24/9/095017

Xu X-J, Deng Z-C, Zhang K, Meng J-M (2016) Surface effects on the bending, buckling and free vibration analysis of magneto-electro-elastic beams. Acta Mech 227:1557–1573. https://doi.org/10.1007/s00707-016-1568-7

Yang F, Chong ACM, Lam DCC, Tong P (2002) Couple stress based strain gradient theory for elasticity. Int J Solids Struct 39:2731–2743. https://doi.org/10.1016/S0020-7683(02)00152-X

Yeh P-C, Chung T-K, Lai C-H, Wang C-M (2016) A magnetic–piezoelectric smart material-structure utilizing magnetic force interaction to optimize the sensitivity of current sensing. Appl Phys A 122:29. https://doi.org/10.1007/s00339-015-9552-y

Zhou Y-H, Gao Y, Zheng XJ (2003) Buckling and post-buckling analysis for magneto-elastic–plastic ferromagnetic beam-plates with unmovable simple supports. Int J Solids Struct 40:2875–2887. https://doi.org/10.1016/S0020-7683(03)00079-9

Zhou S-M, Sheng L-P, Shen Z-B (2014) Transverse vibration of circular graphene sheet-based mass sensor via nonlocal Kirchhoff plate theory. Comput Mater Sci 86:73–78. https://doi.org/10.1016/j.commatsci.2014.01.031